2016

A late Quaternary vertebrate deposit in Kudjal Yolgah Cave, south-western Australia: refining regional late Pleistocene extinctions

Nathan Jankowski
University of Wollongong, nrj934@uowmail.edu.au

Grant A. Gully
Flinders University

Zenobia Jacobs
University of Wollongong, zenobia@uow.edu.au

Richard G. Roberts
University of Wollongong, rgrob@uow.edu.au

Gavin J. Prideaux
Flinders University, gavin.prideaux@flinders.edu.au

A late Quaternary vertebrate deposit in Kudjal Yolgah Cave, south-western Australia: refining regional late Pleistocene extinctions

Abstract

We describe the stratigraphy and chronology of Kudjal Yolgah Cave in south-western Australia, a late Quaternary deposit pre- and post-dating regional human arrival and preserving fossils of extinct and extant fauna. Single-grain optically stimulated luminescence (OSL) dating shows that seven superposed units were deposited over the past 80 ka. Remains of 16 mammal species have been found at the site, all of them represented in Unit 7, for which seven OSL ages indicate accumulation between 80 and 41 ka. Single-grain OSL equivalent dose distribution patterns show no evidence of reworking of older or younger sediments into Unit 7, but late Holocene charcoal has been washed into the top of it from adjacent Unit 2, deposited 1.2 ka ago. Six species that failed to survive the Pleistocene are recorded in Unit 7, but only the south-western wombat Vombatus hacketti is recorded in younger units. Two species, the large extinct kangaroos Protemnodon sp. cf. P. roechus and Procoptodon browneorum, are represented by articulated specimens near the top of Unit 7, immediately adjacent to an OSL sediment sample dated to 41 ± 2 ka. These are the youngest reliably dated records of these genera from mainland Australia, and among the youngest megafaunal remains from the continent. All species currently known from the middle Pleistocene of the south-west persisted into the late Pleistocene, which removes a key pillar supporting the argument against a driving role for human impacts in the extinctions.

Keywords

pleistocene, extinctions, australia, western, south, regional, cave, quaternary, yolgah, kudjal, deposit, vertebrate, refining, late

Publication Details

Jankowski, N. R., Gully, G. A., Jacobs, Z., Roberts, R. G. & Prideaux, G. J. (2016). A late Quaternary vertebrate deposit in Kudjal Yolgah Cave, south-western Australia: refining regional late Pleistocene extinctions. Journal of Quaternary Science, 31 (5), 538-550.

Stratigraphy and chronology of a late Quaternary vertebrate deposit in Kudjal Yolgah Cave, southwestern Australia

NATHAN R. JANKOWSKI,[1 2*] GRANT A. GULLY,[3] ZENOBIA JACOBS,[1] RICHARD G. ROBERTS[1] and GAVIN J. PRIDEAUX[3]

[1]Centre for Archaeological Science, School of Earth & Environmental Sciences, University of Wollongong, Wollongong, NSW 2522, Australia.

[2]Department of Archaeology, Durham University, South Road, Durham DH1 3LE, UK

[3]School of Biological Sciences, Flinders University, Bedford Park, SA 5042, Australia.

* Corresponding author

Ph. (44) 191 334 1576

Current Address: Department of Archaeology, Durham University, South Road, Durham DH1 3LE, UK.

nathan.jankowski@durham.ac.uk

We describe the stratigraphy and chronology of Kudjal Yolgah Cave in southwestern Australia; a late Quaternary deposit preserving fossils of extinct species and post-dating regional human arrival. Single-grain optically stimulated luminescence (OSL) dating shows that seven superposed units were deposited over the past 81 ka. Remains of 16 mammal species have been found at the site, all of them represented in Unit 7, for which seven OSL ages indicate accumulation between 81 and 41 ka ago. While single-grain OSL equivalent dose distribution patterns show no evidence of reworking of older or younger sediments into Unit 7, late Holocene charcoal has been washed into the top of it from the adjacent 1.2 ka old Unit 2. Six species that failed to survive the Pleistocene are recorded in Unit 7, but only the southwestern wombat *Vombatus hacketti* is recorded in younger units. Two species, the large extinct kangaroos *Protemnodon* sp. cf. *P. roechus* and *Procoptodon browneorum*, are represented by articulated specimens near the top of Unit 7, immediately adjacent to an OSL sediment sample dated to 41 ± 2 ka. These are the youngest reliably-dated records of these genera from mainland Australia, and among the youngest megafaunal remains from the continent.

Keywords: OSL, Pleistocene, megafauna, extinction, southwestern Australia

Introduction

The debate over what drove the extinction of >90% of Australia's larger Pleistocene mammals, reptiles and birds remains a very active field of study. As such, a number of models have been proposed to explain this faunal loss. These models include but are not limited to: direct hunting (Flannery, 1990; Brook and Bowman, 2004; Brook and Johnson, 2006), human-mediated ecosystem collapse due to fire (Miller *et al.,* 1999, 2005; Prideaux *et al.,* 2007a) and/or increasingly severe climatic deterioration well before human arrival (e.g., Field *et al.,* 2008; Wroe *et al.,* 2013). To identify the factors responsible, we must, at the very least, establish when species disappeared by applying numerical dating methods to palaeontological remains and associated deposits in a range of geomorphic and ecological settings. While direct dating of fossils using radiocarbon (^{14}C), electron spin resonance and/or uranium–thorium (U–Th) dating methods may be ideal (Gillespie *et al.,* 2006; Turney *et al.,* 2008; Grün *et al.,* 2010), it is sometimes not possible due to diagenetic alteration or loss of datable material preserved within fossils. Moreover, in contrast to other continents, most of the Australian extinctions occurred around or beyond the ca 50 ka limit of ^{14}C dating (Roberts *et al.,* 1994; Bird *et al.,* 1999; Turney *et al.,* 2001; Reimer *et al.,* 2013).

Caves preserve some of the most complete and best-studied archives of Australian Pleistocene vertebrates (e.g., Wells *et al.,* 1984; Roberts *et al.,* 2001; Prideaux *et al.,* 2007a,b, 2010; Turney *et al.,* 2008; Macken *et al.,* 2011; McDowell *et al.,* 2013). Stable-isotopic analyses of faunal remains found within caves can shed light on past environmental changes (e.g., Prideaux *et al.,* 2007a, 2010). Sedimentary infilling of caves often occur at temporally discrete periods, resulting in typically well-stratified deposits (Collcutt, 1979; Straus, 1990; Sherwood and Goldberg, 2001) that provide excellent stratigraphic constraints. When these stratified deposits contain an abundance of quartz grains, the application of OSL dating is an attractive option (e.g., Murray and Roberts, 1997; Darrénougué *et al.,* 2009; Macken *et al.,* 2011). OSL dating provides an estimate of the time elapsed since mineral grains were last exposed to sunlight (Huntley *et al.,* 1985; Aitken, 1998). When applied to deposits containing faunal remains for which taphonomic and lithological evidence suggests minimal or no reworking from older or younger strata, the time elapsed since death can be assumed to be close to the OSL age estimate of the entombing and associated sediments.

Kudjal Yolgah Cave (KYC) rose to prominence more than a decade ago in a continent-wide, multi-grain OSL dating study that argued in favour of an extinction event around 46 ka at the hands of recently-arrived humans (Roberts *et al.,* 2001). KYC yielded one of the two youngest OSL ages from the continent associated with articulated (i.e., clearly non-reworked) specimens of now-extinct Pleistocene vertebrates. However, no detailed site data was or has since been published leading some authors to eliminate KYC from consideration in the extinction debate (Field *et al.,* 2008; 2013). Moreover, the initial reports of OSL ages on quartz grains from KYC (Roberts *et al.,* 2001; Ayliffe *et al.,* 2008) were based on multi-grain aliquots. In this study, we have used single-grain OSL dating, which has a number of inherent benefits over multi-grain OSL techniques (Jacobs and Roberts, 2007; Duller 2008; Roberts *et al.,* 2015). The ability to 1) recognise and reject grains with aberrant physical properties; 2) examine the stratigraphic integrity of the deposit through determination of whether or not the

sediments have been post-depositionally mixed; and 3) assess whether the electron traps were adequately emptied prior to burial ('well' or partially-bleached).

The aim of this paper is to reconstruct the depositional history of KYC by describing its stratigraphy, analysing its sedimentological properties, and applying single-grain OSL dating to the previous samples and a collection of new samples. Together, this study will provide an improved context and age estimates for the remains of relatively late-surviving Pleistocene species.

Geological setting and study area

KYC (34.99° S, 115.05° E; Cave Number 6WI-9) is situated in the Leeuwin–Naturaliste National Park, 5 km southwest of Forest Grove (Fig. 1). It lies within a Pleistocene-aged limestone ridge that stretches from Cape Naturaliste in the north to Cape Leeuwin in the south. This Leeuwin–Naturaliste Ridge forms part of the much larger Tamala Limestone (Playford *et al.,* 1976), which outcrops along the coastal fringe of the Perth and Carnarvon Basins. The Tamala Limestone consists of a series of interbedded aeolian calcarenite and palaeosol facies (Playford *et al.,* 2013). The aeolian calcarenite facies typically contain <10% quartz sand, whereas in the palaeosol facies the quartz-sand fraction is up to 95% (Hearty and O'Leary, 2008; Brooke *et al.,* 2014). The numerous age estimates obtained from various locations and litho-facies within the Tamala Limestone trend younger westward and display episodic construction over successive glacial–interglacial cycles. Hearty and O'Leary (2008) contend that the oldest strata of the Tamala Limestone (such as those containing cavernous weathering features like KYC) were deposited during the early Pleistocene (>780 ka), although this estimate remains to be rigorously tested.

KYC is a stream-derived cavity. The deeper portion of the cave retains an active stream that supports a diverse aquatic root mat of high conservation importance (Jasinska, 1997). Here the Tamala Limestone sits unconformably over impermeable Precambrian-age basement rocks. Numerous caves in the region exhibit past and present surface drainage into vadose underground streams and/or phreatic dissolution of the carbonate along the unconformity interface producing void spaces. This process can form vast caverns when the overlying limestone can no longer be supported. Such caves, including KYC, are typified by arch-shaped ceilings and usually contain large central rock piles of collapsed host rock (Grimes, 2006). They are often linked to the surface by solution pipes, fissures or both, allowing for the episodic infilling of the cave system producing a cone of sediments that laps onto and drapes over the central rock pile.

Previous research

The first recorded collection of fossils from KYC was by a small team from the Western Australian Museum (WAM) led by George W. Kendrick on 21 May 1987. They collected 19 specimens from the site, which were chipped out of a 'fissure fill deposit' (i.e., the blocked solution pipe above the deposit) and collected from the 'modern floor surface'. This

collection was subsequently registered in the Department of Earth and Planetary Sciences, WAM. It includes specimens of *Setonix brachyurus* and *Macropus* sp. indet., and two partial crania initially attributed to *Simosthenurus occidentalis* but later re-identified as belonging to *Procoptodon browneorum* (Prideaux, 2004).

Test excavations each with an approximate volume of 0.2 m^3 were dug in 1994 by amateur palaeontologist Lindsay Hatcher on the north and south sides of the deposit. Specimens collected are now housed in the WAM. Hatcher returned to KYC in April 1997 with one of the authors (RGR) as part of a survey of late Pleistocene deposits in the region. Samples for OSL dating were collected from a small test pit on the north side of the sediment cone (KY1 and KY2), and also beneath a capping flowstone (KY3; Figs. 2 and 3). These gave four U–Th ages ranging from 35.4 ± 0.5 to 33.6 ± 0.8 ka (Roberts *et al.,* 2001). One OSL sample (KY3) collected adjacent to a partial forelimb of *Protemnodon* sp. cf. *P. roechus* was originally dated to 46 ± 2 ka (Roberts *et al.,* 2001), but later redated using the single-grain method to 40 ± 2 ka (Prideaux *et al.,* 2010). No stratigraphic control was maintained during the 1997 collections, but the holes left by the OSL sampling tubes remained and could later be precisely tied to the stratigraphy. Quartz grains adhering to three articulated caudal vertebrae in the Hatcher collection attributed to *Procoptodon browneorum* were dated to 46 ± 6 ka (Table 2 of Roberts *et al.,* 2001, sampled labelled 'Attached to WAM specimen' under heading 'Site 23').

Methods

Excavation and fossil preparation

Systematic excavations at KYC were conducted by a team from Flinders University headed by GJP and GAG in January, September and October 2008. The excavation area was divided into North and South Pits (Figs. 2 and 3). Each pit was then partitioned into ~1 m^2 quadrants, with the precise dimensions of each dictated, and impinged upon, by the surrounding limestone block-fall topography. A track used by cavers and researchers crossed the flowstone originally capping the South Pit, resulting in fragmentation of the flowstone and disturbance of the top 10 cm of underlying sediment (Figs. 2 and 3). More flowstone was removed during our excavation to facilitate excavation of deeper sediments. Clearly disturbed sediment was also removed at the beginning of the 2008 excavations and analysed separately from that which remained *in situ*. At this time, the KY3 OSL sampling hole was relocated and found to still be surrounded by *in situ*, fossiliferous sediment.

Excavations were conducted using standard palaeontological techniques and surveyed using a Total Station (electronic theodolite and laser rangefinder). Excavated sediment was removed from the cave for sieving to recover small bones, teeth and snail shells. Wet sieving was carried out on sediments excavated during the January 2008 field season as a means of obtaining higher yields of small animal remains. However, this intensive and time-consuming practice was not continued in the September–October 2008 field season after it was established that very few small animal remains were preserved in the sediments. As such, dry

sieving was instead conducted due to the negligible difference in specimen yield between these two methods in KYC.

Most specimens required only basic mechanical cleaning to remove sediment encrustation. A 3% acetic acid solution was used to remove calcite-cement coatings from a small proportion of fossil specimens that were more heavily encrusted with sediments. The specimens were then washed to remove any residual acid or salts and allowed to dry. The majority of fossils were strengthened by applying polyvinyl butyrate (Mowital, Clariant) dissolved in 100% ethanol. A select number of specimens from each stratigraphic unit were also hardened complete with sedimentary encrustation to preserve a record of preservation characteristics. All fossils excavated have been registered with the Department of Earth and Planetary Sciences, WAM.

Sediment analysis

Samples collected for OSL dating were subsampled for sediment analysis. Approximately 15 g of sediment was examined for colour using a Munsell Soil Colour Chart (1994). Angularity was assessed under an Olympus binocular microscope. Grain-size analysis was conducted by first immersing samples in 5% hydrochloric acid, which removed any calcium carbonate precipitate that may have cemented grains together. Samples were then allowed to settle for five days, decanted carefully with a syringe, refilled with demineralised water, and again allowed to settle before being decanted to remove salts. After drying, a 1-mm sieve was used to remove grains larger than the sediment analysis machine could accommodate. These were weighted separately. The sediment was then mixed to a thick slurry to ensure larger grains were not preferentially sampled before being analysed in a Malvern Mastersizer 2000 at 3750 rpm, 7–10% obfuscation. Grain-size descriptions used GRADISTAT 8.0 (Blott and Pyne, 2001).

Luminescence sample collection and preparation

Eleven samples were collected for single-grain OSL dating in 2008 to add to the three samples collected by RGR in 1997 (Roberts *et al.,* 2001). Two samples were initially collected in January 2008 (KYC-08n, KYC-08s) from Unit 7, one each from the North and South pits (Figs. 2 and 3). Both were collected by inserting opaque PVC tubes (10 cm in diameter and 20 cm long) into the section. After removal of the tubes, both ends were secured with tissue paper and duct tape. No *in situ* gamma dose rate measurements were collected. A small portion of the light-exposed ends of each tube was removed for water content and laboratory dosimetry measurements. A further nine samples (KY08-1 to KY08-9) were collected under subdued red light conditions in October 2008 using a hand auger. Following the removal of light-exposed grains from the section surface, the auger was used to drill into the sediments and collect the ‘light-safe’ materials beneath. The sediments were double wrapped in black plastic bags for transport to the luminescence laboratory. *In situ* gamma spectrometry measurements, using a two-inch NaI(Tl) gamma detector and measuring the incident gamma radiation for 60 min were made for all KY08 samples (except KY08-2) . Additional sediment removed from inside each sample hole was collected and placed in clear plastic bags for laboratory-based dosimetry measurements, field moisture content estimates

and Munsell colour analysis. For sample KY08-2, a large flowstone at the back of the sample tube hole prevented the insertion of the gamma spectrometer.

This study also presented the opportunity to remeasure the samples that were collected in 1997 (KY1–KY3) by Roberts *et al.* (2001). KY1 and KY2 were collected from a pit on the northern side of the central rock, whereas KY3 was collected from a test pit on the southern side, which was expanded to become the South Pit (Fig. 2).

A full description of OSL sample preparation and measurement and analytical procedures and equipment are provided in Supporting Information. D_e values for individual grains of quartz were determined using a single-aliquot regenerative-dose procedure (e.g., Murray and Wintle, 2000). The effective dose rate to the hydrofluoric acid-etched quartz grains is derived from gamma rays, beta particles, internal alpha particles and cosmic rays. Emission counting methods, including thick-source alpha counting (TSAC), GM-25-5 beta counting and *in situ* gamma spectrometry, were used to determination the environmental dose rates for all samples. Radioactive concentrations and activities were converted to dose rates using the conversion factors of Guérin *et al.* (2011), and cosmic-ray dose rates were estimated following Prescott and Hutton, (1994).

Radiocarbon Samples

Five charcoal samples were collected in September 2008 by GJP and submitted to the Oxford Radiocarbon Accelerator Unit for ^{14}C AMS dating using the procedures of Brock *et al.,* (2010). Ages were reported in Bronk Ramsey *et al.* (2015). Four samples were collected from sediment 0–20 cm below the flowstone that cap the south side of the deposit, and one sample was retrieved from the North Pit.

Results

Stratigraphy and sedimentology

Fossil-bearing sediments drape the apex of the rock pile near the top of the main chamber (Figs. 2 and 3). This is located 5 m from the base of the current solution pipe entrance, which is approximately 1.5 x 2 m^2 wide and 4 m deep. A large limestone block forms a central east–west-oriented ridge that divides the chamber into a northern and a southern sector. A blocked solution tube is positioned directly above the deposit. The height of the ceiling varies between 1 and 2 m. Much of the chamber walls are covered with moonmilk. In places fossil bones protrude from the moonmilk-covered sediment adhering to the ceiling, the source for the fossil samples collected by Kendrick *et al.* in 1987. The northern sector, however, is marked by concentrations of stalactites. KYC contains no evidence of human occupation, likely due at least in part to the unsuitable nature of the former and current solution pipe entrances.

Seven Units were recognised during the 2008 excavations; Unit 1 is stratigraphically the highest and Unit 7 the lowest (Fig. 3). Judging from the position of the blocked solution pipe

and the slope of the cone, Units 7–3 accumulated by washing or falling in through this entrance, while Units 2–1 accumulated via the current entrance. All units are composed of highly-friable, medium to very coarse sands with predominantly rounded grains. A complete breakdown of the sedimentological results can be found in the accompanying Supplementary Information. Colour varies between units, although most samples fall within the Munsell (1994) Yellow-Red hue.

Only Units 7 and 2 were intersected in the South Pit. Unit 7 was excavated to a depth of 1.25 m, but more fossil-bearing sediment remains unexcavated below. It is a rounded, coarse to very coarse sand showing a subtle gradation in sediment colour (orange–brown) and the presence of mottling, with the mottle intensity and colour increasing with depth down profile. A colour value of 7.5YR 4/4 (Brown) was measured for two samples taken towards the top of the Unit (near KYC-08s and KY08-2), whereas values of 7.5YR 6/6 (Reddish yellow: KY08-3), 5/4 (Brown:KY08-4) and 6/4 (Strong Brown: KY08-5) were measured closer towards the current excavated level of Unit 7. Unit 7 is capped by the 3 cm-thick flowstone, U–Th-dated from 35.4 ± 0.5 to 33.6 ± 0.8 ka (Roberts *et al.,* 2001). Unit 2 overlies Unit 7 more proximally to the current cave entrance and is separated from it by a distinct angular unconformity due to its accumulation via the current, rather than the blocked, entrance. It thins distally from the current entrance where it onlaps the dated flowstone. Unit 2 is darker in colour than Unit 7 (10YR 4/2: Dark greyish brown) and contains abundant charcoal fragments and land-snail shells.

Units 7–3 and 1 were encountered in the North Pit and filled a 3-m^3 cavity atop the fallen roof blocks. Here, Unit 7 is 25 cm thick, dips more gently than in the South Pit, and rests directly on a flowstone floor. The top of Unit 7 is compacted. The flowstone appears to directly cap fallen limestone blocks. Unit 7 has a strong brown Munsell colour (7.5YR 5/6 for KY08-8 and KYC-08n). Unit 6 (thickness 10 cm) overlies Unit 7, and is in turn capped by Unit 5, an equally thick, compacted moonmilk layer. Units 4 (20 cm thick, 7.5YR 5/4: Brown) and 3 (40 cm thick, 7.5YR 4/4:Brown) lie between Unit 5 and a capping flowstone, and dip away from the central rock pile. Unit 1 caps the deposit. It is still actively accumulating through the current entrance and contains mostly plant debris and charcoal. Relocation of Hatcher's 1994 pit confirms that it cut into and sampled from all Units near the centre of North Pit quadrant A (Fig. 2).

Palaeontology

Remains of 16 mammal species were retrieved during the 2008 excavations (Table 1), along with some indeterminate small reptile and bird fragments. All species represented in the Kendrick and Hatcher collections are present in our stratigraphically excavated sample. Vertebrate remains were collected from Units 2, 5, 6 and 7. Units 1, 6 and 7 produced snail shells (*Bothriembryon sayi, Luinodiscus* sp. indet.). Degree of bone completeness is variable; some bones are well-preserved and relatively complete, but most are fragmentary. Articulated and associated remains were retrieved from Unit 7. The articulated specimens included much of the left and right forelimbs of a specimen of *Protemnodon* sp. cf. *P. roechus* (WAM 08.8.544 / 08.8.587 / 08.8.979 / 08.8.998), which directly abutted the sampling tube for KY3,

and a hind foot and six caudal vertebrae of *Procoptodon browneorum* (WAM 08.8.583). This was collected from the same level, 15–30 cm away. Elements of both specimens were originally collected by Hatcher, including the *P. browneorum* caudal vertebrae reported in Roberts *et al.* (2001).

A significant proportion of fossils retrieved from Unit 7 were encrusted with calcified sand, particularly those collected from closer to the central limestone ridge in the South Pit, where they were exposed to more carbonate-saturated water as they sat buried in sandy sediment. Most bones from Units 2, 5 and 6 had no such patina.

Small-bodied vertebrate species are very poorly represented in the deposit (Table 1). A dentary of *Notomys* sp. cf. *N. mitchellii* from Unit 7 is the only rodent specimen represented by more than a loose incisor. The bandicoots *Perameles bougainville* and *Isoodon obesulus* are known from a total of only five identifiable specimens. Of the 180 registered mammal specimens (i.e., specimens identifiable to at least genus level), 142 (79%) belong in one of four macropodid species: *Macropus fuliginosus* (69 specimens), *M. irma* (19), *Setonix brachyurus* (22) and *Procoptodon browneorum* (32). The heaviest species represented in the deposit is *Protemnodon* sp. cf. *P. roechus* (Table 1), and the remains include those of at least one adult specimen.

At least half of the total volume of sediment excavated from KYC comes from Unit 7, which produced 112 of the 180 registered mammal specimens. Not surprisingly, it yielded the highest number of species, 13 out of the total of 16 mammal species (Table 1). By comparison, Unit 6 produced remains of only two species (*Macropus fuliginosus, Procoptodon browneorum*). There was also a partial cranium of *Vombatus hacketti* embedded in Unit 5, the thick moonmilk layer overlying Unit 6. Units 3 and 4 yielded no fossils. Unit 2 produced three species and Unit 1 four species (Table 1). Remains of the three species recorded from the site but not from Unit 7 (*Simosthenurus pales, Bettongia penicillata, Pseudocheirus occidentalis*) were retrieved only from disturbed sediments. Sample sizes from all of the Units are presently too low to detect temporal changes in regional faunal composition.

Luminescence chronology

The D_e values for all accepted grains from all samples are displayed, in stratigraphic order, as radial plots in Fig. S4. Two example radial plots for samples KY3 and KY08-6 are presented in Fig. 4a and b. A total of 10,900 grains were measured for all 14 samples, but only 4,025 grains (37% of the total) passed the rejection criteria (Table S2). Table 2 contains information about the number of grains used for D_e determination, the D_e overdispersion values and the modelled D_e estimate used to calculate the age of each sample.

Visual inspection of radial plots suggests two different types of D_e distributions (Figs. 7 and 8). We hypothesise that not all grains experienced similar burial histories, and that two different site formation processes were involved in the accumulation of the KYC deposit.

Nine samples have D_e distributions consistent with grains that are thought to have been well-bleached prior to burial (Fig. 4a; Fig. S4 in SI), including all of those from Unit 7. The calculated OD values for these samples range between 20 ± 1 and 32 ± 2%. Radial plots of these samples reveal log D_e values spread more-or-less symmetrically around the central D_e value (Fig. 4a). The presence of articulated fossil remains in the associated deposits argues against significant post-depositional mixing. We infer that the larger-than-expected-spread in D_e values is likely the result of small-scale differences in the beta dose rate received by the individual grains. Accordingly, the CAM of Galbraith *et al.* (1999) was used to obtain the D_e values for these samples. The close agreement of the OSL ages of these samples with independent age control (e.g., U–Th ages from the capping flowstone) suggests that it is reasonable to infer that such distributions are typical of well-bleached grains that remained undisturbed after burial.

The remaining five KYC samples display D_e patterns characteristic of partially bleached samples (Fig. 4b; Fig. S4 in SI; Olley *et al.,* 1999; 2004b). However, in this karstic environment a two-stage depositional phase is proposed. It is considered that a population of well-bleached grains were first delivered into the cave. This was then followed by the transportation of these sediment further into the cave system and also saw the incorporation of pre-existing (i.e., dosed) sediment in the darkness of the cave. These processes result in radial plots that display a conspicuous clustering of D_e values at the minimum dose, with a continuous spread in D_e values to higher doses (e.g., >130 Gy) and OD values between 29 ± 2 and 85 ± 8%. For such distributions, the smallest values within each sample will more likely correspond to the time of deposition of the most recently bleached grains (i.e., the grain population considered most representative of the final depositional age). To estimate this burial dose, the minimum age model (MAM) of Galbraith *et al.* (1999) was used with a relative uncertainty of 20% (added in quadrature to each of the D_e measurement uncertainties before running the model). This additional error represents the minimum OD present in the D_e distribution of the samples that were thought to be well-bleached prior to burial.

The calculated total environmental dose rates range between 1.07 ± 0.04 and 1.55 ± 0.13 Gy/ka (Table 2). Those with the highest total dose rates (KY08-2 and KYC-08n) had their gamma dose rate measured using a combination of thick source alpha counting and beta counting. These values are conspicuously higher than those measured for the same unit using an *in situ* gamma spectrometer. The deposits are very inhomogeneous with the presence of low radioactivity flowstone and limestone roof spall, making *in situ* measurement of the gamma dose rate an essential requirement. The validity and usefulness of the gamma dose rates for these samples should be questioned. Similar differences in the gamma dose rate is observed for KY1, KY2 and KY3 when the radioactivity of the sediment only is measured using high resolution gamma spectrometry compared to *in situ* gamma spectrometry (see Table S4 in SI for details of the radionuclides).

The 14 single-grain OSL ages range from 86.7 ± 5.9 ka (KY08-9) for a sample of sediment adhering to the ceiling immediately above the deposit, to 1.2 ± 0.1 ka for Unit 2 (Figs. 2 and 3; Table 2). The age estimate for KY08-9 is statistically consistent with the age estimate of the samples collected from the deepest excavated portion of Unit 7 in the South Pit – 80.5 ±

5.0 ka (KY08-3). The remaining ages for samples from Unit 7 in the South Pit are successively younger, from 64.6 ± 3.9 ka (KY08-4) collected 10 cm above KY08-3 to 41.4 ± 1.9 ka (KY3) collected 30 cm below the flowstone. OSL ages of 67.1 ± 4.3 (KY08-8) and 53.3 ± 4.9 ka (KY-08n) were obtained for the two samples collected form Unit 7 in the North Pit. An age of 21.3 ± 1.2 ka (KY1) was obtained for Unit 6. Samples collected from Unit 4 gave ages of 6.9 ± 0.5 ka (KY08-7) and 7.7 ± 0.4 ka (KY2). The overlying Unit 3 produced an age of 5.8 ± 0.4 ka (KY08-6). Sample KY08-1, collected from Unit 2 in the South Pit, is the youngest sample measured in this study, yielding an OSL age of 1.2 ± 0.1 ka.

Radiocarbon chronology

Four charcoal clasts (OxA-23686 to OxA-23689) collected from within the top 20 cm of Unit 7, beneath the flowstone, produced ^{14}C AMS ages (Table 3) ranging from 1 258 ± 26 to 904 ± 25 cal BP (Bronk-Ramsey *et al.,* 2015). These are much younger than the U–Th age of 35–34 ka for the underlying flowstone and the OSL ages of ≥40 ka for Unit 7. They are, however, concordant with the OSL age of 1.2 ± 0.1 ka on the charcoal-rich Unit 2, which cuts across Unit 7 (Figs 1–2). The ^{14}C AMS age of 4 566 ± 32 cal BP on charcoal collected from Unit 6 is distinctly younger than the OSL age of 21 ± 1 ka (Table 2).

The most parsimonious explanation for the 1.2–0.9 ka ^{14}C ages for charcoal from the top of Unit 7 is that the charcoal was reworked from the adjacent Unit 2. Settling over time led to compaction of the sediment composing Unit 7, resulting in a gap of approximately 5 cm between the flowstone and the top of Unit 7. Smaller, lighter charcoal clasts were washed into the gap under the flowstone and scoured into the highly friable sand. Because charcoal is light and easily transported by water, it may be more commonly reworked in cave settings than is frequently perceived (Archer, 1974; Carcaillet *et al.,* 2007). This hypothesis is supported by the D_e distributions of the Unit 7 samples (Fig. 4a and Fig. S4), which show no characteristics associated with mixing (cf. David *et al.,* 2007). Similarly, the ^{14}C age of 4.5 ka cal B.P. on charcoal from Unit 6 is discordant with the OSL age of 21 ka. How the charcoal was reworked into Unit 6 is not clear. The deposit is penetrated today, and presumably has in the past been penetrated by multiple roots of Karri (*Eucalyptus diversicolor*), and so transport down a root hole is a possibility. These examples highlight a further advantage of analysing multiple single-grain OSL samples as a primary chronological method in cave settings.

Discussion

Site depositional history

Fossils and sediment dated to 87 ± 6 ka adhering to the ceiling represent an initial phase of accumulation. We hypothesise that, at this time, this part of KYC was composed of a small chamber overlying a larger chamber. Fauna and sediments were deposited via the overhead solution pipe (Fig. 3) for an unknown duration, but terminated at 87 ± 6 ka when the shallow, higher chamber filled to the ceiling, blocking the solution pipe. The floor of this chamber

then collapsed into the underlying chamber, unblocking the solution pipe and allowing sediment and faunal accumulation to recommence onto the rock pile produced from the collapse. That deposition was reinitiated relatively promptly is supported by the overlapping errors on the mean age of the ceiling sediment and the oldest age for Unit 7 (80 ± 5 ka).

Lithological and chronological evidence from Unit 7 suggests that sediment accumulation began around 80 ka ago and terminated with blockage of the solution pipe around 40 ka ago. D_e distributions for Unit 7 sediment are consistent with grains having been well-bleached at the time of deposition, further supporting the interpretation that they entered through the overhead solution pipe. Whether deposition of Unit 7 was gradual or intermittent cannot currently be verified. The lack of any indicative break in clastic deposition, such as compacted moonmilk or flowstone layers, within Unit 7 suggests that the former is more likely. In contrast, the gradual shift in colour, from orange-brown mottled at the base to less mottled at the top of Unit 7, may reflect either a poorly-developed weathering profile, given the protracted period of accumulation, or two depositional phases. Examination of the gamma dose rates (Table 2) for the samples collected from this unit may provide evidence for this. If we consider that the gamma dose rate estimates determined for three samples from this unit (KYC-08s, KYC-08n, KY08-2) using TSAC are overestimates of the 'true' gamma dose (as the gamma spectrometer measurements for the remaining samples are, on average, half of that of the TSAC determinations), then the resulting age estimates would underestimate the true burial age of the sediment. It could be inferred that two depositional episodes (one at ~60 ka and another at ~40 ka) may have taken place. The Unit 7 capping flowstone precipitated at 35–34 ka ago.

The solution pipe unblocked at around 21 ka ago, facilitating the phase of sediment infilling that produced Unit 6. This is capped by Unit 5, a thick moonmilk layer that accumulated via roof spall during another interval of solution-pipe closure. The fossil wombat skull embedded in Unit 5 must have lain on the surface of Unit 6 as the pipe blocked again. These remains are analogous to the fossil material embedded in Unit G in the nearby Tight Entrance Cave (Ayliffe *et al.,* 2008; Prideaux *et al.,* 2010). A further phase of sediment infilling in KYC occurred at around 8–6 ka with the deposition of Units 4–3. The absence of fossils from either layer suggests that the pipe aperture was so restricted that only sediment was able to filter into this area of the cave before it became completely blocked. This process would have reduced lighting conditions in the cave and may explain why D_e distributions consistent with 'partially bleached' D_e distributions characterise the post-21 ka sediments in KYC (Fig. 4b).

By 1.2 ka the original solution pipe had blocked completely and sediment began to enter the cave via the current solution pipe entrance (Figs. 2 and 3). The sediments of Unit 2 were washed into the southwest of the central rock pile, thinning out and onlapping the flowstone capping the southeast corner of the cone. The charcoal-rich nature of Unit 2 may indicate that the opening of the current entrance was, at least in part, facilitated by a bushfire. A natural or anthropogenic shift on the western edge of the rock pile apex resulted in a switch in the flow of sediments and debris into the cave from the south side (Unit 2) to the north side of the cone (Unit 1) on either side of a depositional hiatus of perhaps 1 ka. Unit 1 is still accumulating via the current entrance.

Faunal evidence

The KYC deposit shows that at least six species failed to survive the Pleistocene in southwestern Australia. Among them, the kangaroos *Procoptodon browneorum* and *Protemnodon* sp. cf. *P. roechus* were still extant at 40 ka, as indicated by articulated remains collected from near the top of Unit 7. Their age is further constrained by subjacent OSL ages of 46 and 55 ka. We interpret a partial cranium of *Vombatus hacketti* from Unit 5 as *in situ*; it sat on the surface of Unit 6, which is dated to 21 ka, and then became encased in moonmilk (Unit 5) after the solution pipe closed. The isolated incisor of *P. browneorum* retrieved from Unit 6 (21 ka) cannot be confirmed as *in situ*. It could feasibly have sat on the surface of Unit 7 and been reworked into the base of Unit 6. Remains of *Simosthenurus occidentalis* and *Thylacoleo carnifex* from Unit 7 have a maximum age of 80 ka. The oldest age for the deposit, 87 ka on sediment adhering to the ceiling, provides a maximum age for a specimen of *Simosthenurus pales*, because its precise stratigraphic provenance is unknown. Each of these six species are represented in the nearby Tight Entrance Cave deposit by specimens aged around 50 ka or younger (Prideaux *et al.,* 2010). Thus, although the KYC record adds no new species to the list of late Pleistocene survivors in the southwest, it strongly reinforces the existing evidence that several larger species remained extant when humans first arrived in the region.

Conclusion

Here, 7 stratigraphic units are reported in conjunction with 14 single-grain OSL and 5 radiocarbon ages. A total of 16 species of mammal, including 6 megafaunal species, were identified from Unit 7 of the KYC deposit, which accumulated between 80 ± 5 and 40 ± 2 ka based on the single-grain OSL chronology. The D_e distribution patterns for the 8 samples from this unit suggest that that it is comprised of sediment that were well-bleached at deposition and have not suffered from post-depositional mixing subsequent to burial. The erroneously young ^{14}C ages for charcoal recovered from this same unit (1300–900 cal BP) are considered to be intrusive and not associated with the deposition of Unit 7. With the exception of *Vombatus hacketti*, which survived to ~17 ka, the fossil remains for the remaining five megafaunal species fossils are older than 40 ± 2 ka ago. This finding mirrors similar trends observed at other cave locations within the region.

Acknowledgements – We thank the volunteers, students, colleagues and friends who helped with excavations in KYC, particularly Anthony O'Flaherty for surveying. Funding and/or logistic support was provided by the Australian Research Council (DP0772943), Western Australian Department of Parks and Wildlife (formerly Environment and Conservation), Augusta–Margaret River Tourism Association and Western Australian Museum. Z.J., R.G.R. and G.J.P. are supported by an Australian Research Council Queen Elizabeth II Fellowship

(DP1092843), a Laureate Fellowship (FL130100116) and a Future Fellowship (FT130101728), respectively.

References

Aitken MJ. 1998. *An introduction to optical dating: the dating of Quaternary sediments by the use of photon–stimulated luminescence*. Oxford University Press, Oxford.

Archer M. 1974. Apparent association of bone and charcoal of different origin and age in cave deposits. *Memoirs of the Queensland Museum* **17** : 37–48.

Ayliffe LK, Prideaux GJ, Bird MI, Grün R, Roberts RG, Gully GA, Jones R, Fifield LK, Cresswell RG 2008. Age constraints on Pleistocene megafauna at Tight Entrance Cave in southwestern Australia. *Quaternary Science Reviews* **27** : 1784–1788.

Blott SJ, Pye K. 2001. GRADISTAT: a grain size distribution and statistics package for the analysis of unconsolidated sediments. *Earth Surface Processes and Landforms.* **26** : 1237–1248.

Bronk Ramsey C, Higham TFG, Brock F, Baker D, Ditchfield P, Staff RA. 2015. Radiocarbon dates from the Oxford AMS System: Archaeometry Datelist 35. *Archaeometry* **57** : 177–216.

Brook BW, Bowman DMJS. 2004. The uncertain blitzkrieg of Pleistocene megafauna. *Journal of Biogeography* **31** : 517–523.

Brook BW, Johnson CN. 2006. Selective hunting of juveniles as a cause of the imperceptible overkill of the Australian Pleistocene megafauna. *Alcheringa Special Issue* **1** : 39–48.

Brooke BP, Olley JM, Pietsch T, Playford PE, Haines PW, Murray-Wallace CV, Woodroffe CD. 2014. Chronology of Quaternary coastal aeolianite deposition and the drowned shorelines of southwestern Western Australia – a reappraisal. *Quaternary Science Reviews* **93** : 106–124.

Carcaillet C, Perroux A-S, Genries A, Perrette Y. 2007. Sedimentary charcoal pattern in a karstic underground lake, Vercors massif, French Alps: implications for palaeo-fire history. *The Holocene* **17** : 845–850.

Collcutt SN. 1979. The Analysis of Quaternary Cave Sediments. *World Archaeology* **10** : 290–301.

Darrénougué N, De Deckker P, Fitzsimmons KE, Norman MD, Reed L, van der Kaars S, Fallon S. 2009. A late Pleistocene record of aeolian sedimentation in Blanche Cave, Naracoorte, South Australia. *Quaternary Science Reviews* **28** : 2600–2615.

David B, Roberts RG, Magee J, Mialanes J, Turney C, Bird M, White C, Fifield LK, Tibby J. 2007. Sediment mixing at Nonda Rock: investigations of stratigraphic integrity at an early archaeological site in northern Australia and implications for the human colonisation of the continent. *Journal of Quaternary Science* **22** : 449–479.

Duller GAT. 2008. Single-grain optical dating of Quaternary sediments: why aliquot size matters in luminescence dating. *Boreas* **37** : 589–612.

Field J, Fillios M, Wroe S. 2008. Chronological overlap between humans and megafauna in Sahul (Pleistocene Australia–New Guinea): A review of the evidence. *Earth-Science Reviews* **89** : 97–115.

Field J, Wroe S, Trueman CN, Garvey J, Wyatt-Spratt S. 2013. Looking for the archaeological signature in Australian megafaunal extinctions. *Quaternary International* **285** : 76–88.

Flannery TF. 1990. Pleistocene faunal loss: implications of the aftershock for Australia's past and future. *Archaeology in Oceania* **25** : 45–55.

Galbraith RF, Roberts RG, Laslett GM, Yoshida H, Olley JM. 1999. Optical dating of single and multiple grains of quartz from Jinmium rock shelter, Northern Australia: Part I, experimental design and statistical models. *Archaeometry* **41** : 339–364.

Gillespie R, Brook BW, Baynes A. 2006. Short overlap of humans and megafauna in Pleistocene Australia. *Alcheringa Special Issue* **1** : 163–186.

Goldberg P, Sherwood SC. 2006. Deciphering human prehistory through the geoarcheological study of cave sediments. *Evolutionary Anthropology* **15** : 20–36.

Grimes KG. 2006. Syngenetic Karst in Australia: A Review. *Helictite* **39** : 27–38.

Grün R, Eggins S, Aubert M, Spooner N, Pike AWG, Müller W. 2010. ESR and U-series analyses of faunal material from Cuddie Springs, NSW, Australia: implications for the timing of the extinction of the Australian megafauna. *Quaternary Science Reviews* **29** :596–610.

Guérin G, Mercier N, Adamiec G, 2011. Dose-rate conversion factors: update. *Ancient TL* **29** : 5–8.

Hearty PJ, O'Leary MJ. 2008. Carbonate eolianites, quartz sands, and Quaternary sea-level cycles, Western Australia: A chronostratigraphic approach. *Quaternary Geochronology* **3** : 26–55.

Huntley DJ, Godfrey-Smith DI, Thewalt MLW. 1985. Optical dating of sediments. *Nature* **313** :105–107.

Jacobs Z, Roberts RG. 2007. Advances in optically stimulated luminescence dating of individual grains of quartz from archeological deposits. *Evolutionary Anthropology* **16** : 210–223.

Jasinska EJJ. 1997. *Faunae of aquatic root mats in caves of southwestern Australia: origins and ecology.* PhD Thesis, Department of Zoology, University of Western Australia, Perth.

Macken AC, Jankowski NR, Price GJ, Bestland EA, Reed EH, Prideaux GJ, Roberts RG. 2011. Application of sedimentary and chronological analyses to refine the depositional context of a Late Pleistocene vertebrate deposit, Naracoorte, South Australia. *Quaternary Science Reviews* **30** : 2690–2702.

McDowell MC, Bestland EA, Bertuch F, Ayliffe LK, Hellstrom JC, Jacobsen GE, Prideaux GJ. 2013. Chronology, stratigraphy and palaeoenvironmental interpretation of a Late Pleistocene to mid-Holocene cave accumulation on Kangaroo Island, South Australia. *Boreas* **42** : 974–994.

Miller GH, Fogel ML, Magee JW, Gagan MK, Clarke SJ, Johnson BJ. 2005. Ecosystem collapse in pleistocene Australia and a human role in megafaunal extinction. *Science* **309** : 287–290.

Miller GH, Magee JW, Johnson BJ, Fogel ML, Spooner NA, McCulloch MT, Ayliffe LK. 1999. Pleistocene extinction of Genyornis newtoni: Human impact on Australian megafauna. *Science* **283** : 205–208.

Murray AS, Roberts RG. 1997. Determining the burial time of single grains of quartz using optically stimulated luminescence. *Earth and Planetary Science Letters* **152** : 163–180.

Murray AS, Wintle AG. 2000. Luminescence dating of quartz using an improved single-aliquot regenerative-dose protocol. *Radiation Measurements* **32** : 57–73.

Olley JM, Caitcheon GG, Roberts RG. 1999. The origin of dose distributions in fluvial sediments, and the prospect of dating single grains from fluvial deposits using optically stimulated luminescence. *Radiation Measurements* **30** : 207–217.

Olley JM, Pietsch T, Roberts RG. 2004b. Optical dating of Holocene sediments from a variety of geomorphic settings using single grains of quartz. *Geomorphology* **60** : 337–358.

Playford PE, Cockbain AE, Berry PF, Roberts AP, Haines PW, Brook BP. 2013. The geology of Shark Bay. *Geological Survey of Western Australia Bulletin* **146** : 281 pp.

Playford PE, Cockbain AE, Low GH. 1976. Geology of the Perth Basin, Western Australia. *Western Australia Survey Bulletin.*

Prescott JR, Hutton JT. 1994. Cosmic ray contributions to dose rates for luminescence and ESR dating: large depths and long-term time variations. *Radiation Measurements* **23** : 497–500.

Prideaux GJ. 2004. Systematics and evolution of the sthenurine kangaroos. *University of California Publications in Geological Sciences* **146** : 1–623.

Prideaux GJ, Ayliffe LK, DeSantis LRG, Schubert BW, Murray PF, Gagan MK, Cerling TE. 2009. Extinction implications of a chenopod browse diet for a giant Pleistocene kangaroo. *Proceedings of the National Academy of Sciences of the United States of America* **106** : 11646–11650.

Prideaux GJ, Gully GA, Couzens AMC, Ayliffe LK, Jankowski NR, Jacobs Z, Roberts RG, Hellstrom JC, Gagan MK, Hatcher LM. 2010. Timing and dynamics of Late Pleistocene mammal extinctions in southwestern Australia. *Proceedings of the National Academy of Sciences* **107** : 22157–22162.

Prideaux GJ, Long JA, Ayliffe LK, Hellstrom JC, Pillans B, Boles WE, Hutchinson MN, Roberts RG, Cupper ML, Arnold LJ, Devine PD, Warburton NM. 2007a. An arid-adapted middle Pleistocene vertebrate fauna from south-central Australia. *Nature* **445** : 422–425.

Prideaux GJ, Roberts RG, Megirian D, Westaway KE, Hellstrom JC, Olley JI. 2007b. Mammalian responses to Pleistocene climate change in southeastern Australia. *Geology* **35** : 33–36.

Roberts RG, Flannery TF, Ayliffe LK, Yoshida H, Olley JM, Prideaux GJ, Laslett GM, Baynes A, Smith MA, Jones R, Smith BL. 2001. New ages for the last Australian megafauna: Continent-wide extinction about 46,000 years ago. *Science* **292** : 1888–1892.

Roberts RG, Jacobs Z, Li B, Jankowski NR, Cunningham AC, Rosenfeld AB. 2015. Optical dating in archaeology: thirty years in retrospect and grand challenges for the future. *Journal of Archaeological Science* **56** :41–60.

Sherwood SC,Goldberg P. 2001. A geoarchaeological framework for the study of karstic caves sites in the eastern woodlands. *Midcontinental Journal of Archaeology* **26** : 145–167.

Straus LG. 1990. Underground Archaeology: Perspectives on Caves and Rockshelters. In *Archaeological Method and Theory*, Schiffer MB (ed). University of Arizona Press, Tucson; 255–304.

Turney CSM, Flannery TF, Roberts RG, Reid C, Fifield LK, Higham TFG, Jacobs Z, Kemp N, Colhoun EA, Kalin RM, Ogle N. 2008. Late-surviving megafauna in Tasmania, Australia, implicate human involvement in their extinction. *Proceedings of the National Academy of Sciences USA* **105** : 12150–12153.

Wells RT, Moriarty K, Williams DLG. 1984. The fossil vertebrate deposits of Victoria Fossil Cave Naracoorte: an introduction to the geology and fauna. *The Australian Zoologist* **21** : 305–333.

Wroe S, Field JH, Archer M, Grayson DK, Price GJ, Louys J, Faith JT, Webb GE, Davidson I, Mooney SD. 2013. Climate change frames debate over the extinction of megafauna in Sahul (Pleistocene Australia-New Guinea). *Proceedings of the National Academy of Sciences USA* **110** : 8777–8781.

Table 1. Vertebrate list for Kudjal Yolgah Cave deposit. Body masses are estimated from those values presented in Prideaux *et al.* (2010). Species that become extinct during the Pleistocene are denoted by (†), with the exception of *Phascolarctos cinereus*, which became extinct locally only.

Species	Body mass (kg)	KUDJAL YOLGAH CAVE				
		Unit 7	Unit 6	Unit 5	Unit 2	Unit 1
Thylacinus cynocephalus	25	x				
Dasyurus geoffroii	1.1	x				
Isoodon obesulus	0.78	x				
Perameles bougainville	0.23	x			?	x
Trichosurus vulpecula	4.0	x			x	x
Bettongia lesueur	0.68	x				
Macropus fuliginosus	49	x	x		?	x
Macropus irma	8.0	x				x
Setonix brachyurus	3.0	x				x
Notomys sp. cf. *N. mitchelli*	0.05	x				
Phascolarctos cinereus†	8.0	x				
Vombatus hacketti†	26	x		x		
Thylacoleo carnifex†	104	x				
Protemnodon sp. cf. *P. roechus*†	166	x				
Procoptodon browneorum†	60	x	x			
Simosthenurus occidentalis†	118	x				

Table 2. Dose rates, D_e values and OSL ages of sediment samples from Kudjal Yolgah Cave.

Sample	Unit	Moisture content (%)[1]	Dose rate (Gy/ka)			Total dose rate (Gy/ka)[5]	D_e (Gy)[6]	Used / measured grains (N)	OD (%)[7]	OSL age (ka)[8]
			Beta[2]	Gamma[3]	Cosmic[4]					
KY08-1	2	5.2	0.59 ± 0.04	0.48 ± 0.02	0.13 ± 0.01	1.23 ± 0.07	1.5 ± 0.1[#]	62 / 900	85 ±8	1.2 ± 0.1
KY08-6	3	2.3	0.67 ± 0.04	0.50 ± 0.03	0.13 ± 0.01	1.33 ± 0.07	7.6 ± 0.2[#]	267 / 900	72 ± 3	5.8 ± 0.4
KY2	4	3.5	0.69 ± 0.03	0.42 ± 0.02[γ]	0.13 ± 0.01	1.27 ± 0.04	9.8 ± 0.4[#]	174 / 500	62 ± 4	7.7 ± 0.4
KY08-7	4	1.8	0.68 ± 0.05	0.43 ± 0.02	0.13 ± 0.01	1.27 ± 0.07	8.8 ± 0.3[#]	360 / 900	78 ± 3	6.9 ± 0.5
KY1	6	3.0	0.55 ± 0.03	0.36 ± 0.01[γ]	0.13 ± 0.01	1.07 ± 0.04	22.8 ± 0.9[#]	178 / 500	36 ± 2	21.3 ± 1.2
KY3	7	3.6	0.51 ± 0.03	0.39 ± 0.01[γ]	0.13 ± 0.01	1.07 ± 0.04	44.2 ± 0.9	205 / 500	25 ± 2	41.4 ± 1.9
KY08-2	7	2.0	0.78 ± 0.04	0.61 ± 0.05[α]	0.13 ± 0.01	1.55 ± 0.09	72.2 ± 1.1	421 / 900	23 ± 1	46.5 ± 3.1
KYC-08n	7	1.6	0.68 ± 0.04	0.71 ± 0.09[α]	0.13 ± 0.01	1.55 ± 0.13	82.8 ± 2.7	144 / 400	31 ± 2	53.3 ± 4.9
KYC-08s	7	2.6	0.66 ± 0.04	0.52 ± 0.04[α]	0.13 ± 0.01	1.34 ± 0.09	77.5 ± 1.5	430 / 900	32 ± 2	57.8 ± 4.2
KY08-5	7	2.1	0.83 ± 0.05	0.23 ± 0.01	0.12 ± 0.01	1.22 ± 0.06	75.5 ± 1.1	354 / 900	21 ± 1	62.1 ± 3.7
KY08-4	7	2.3	0.82 ± 0.05	0.31 ± 0.02	0.12 ± 0.01	1.29 ± 0.07	83.4 ± 1.5	293 / 800	23 ± 1	64.6 ± 3.9
KY08-8	7	2.5	0.67 ± 0.04	0.25 ± 0.01	0.13 ± 0.01	1.08 ± 0.06	72.7 ± 1.4	361 / 900	28 ± 1	67.1 ± 4.3
KY08-3	7	1.4	0.60 ± 0.04	0.33 ± 0.02	0.13 ± 0.01	1.09 ± 0.06	87.5 ± 1.2	388 / 900	20 ± 1	80.5 ± 5.0
KY08-9	roof	3.5	0.32 ± 0.02	0.11 ± 0.01	0.13 ± 0.01	0.59 ± 0.04	51.4 ± 0.9	384 / 1000	32 ± 1	86.7 ± 5.9

1. *In situ* gamma spectrometry measurements were made at field water content (1.2–5.2%). Beta counting and thick-source alpha counting measurements were made on dried and powdered sediment samples. All dose rate components were then calculated for a water content of 5 ± 2 %. This value and uncertainty were chosen as they encompass the range of the present-day water contents and are likely to accommodate past water contents at 2σ. Field water content was calculated as the mass of water divided by the mass of dry sample, expressed as a percentage.
2. Mean ± standard error. Determined by beta counting for all samples using the procedures and equipment described in Jacobs & Roberts (2015).
3. Mean ± standard error. *In situ* gamma dose rates using the 2-inch detector for all samples, except for those denoted with (^{γ}) and (^{α}) which were determined with the 3-inch gamma detector and a combination of thick-source alpha counting and beta counting, respectively.
4. Calculated cosmic dose rate using the equations of Prescott & Hutton (1994) using a latitude of 34° south, a longitude of 155° east, an altitude of 50 m, sediment and rock densities of 2.0 g cm-3 and 1.2 g cm-3, respectively, and a constant rock overburden thickness of 5 m. 10% (1σ) uncertainty applied to each estimated value.
5. Mean ± total (1σ) uncertainty, calculated as the quadratic sum of the random and systematic uncertainties. The total dose rates include an internal alpha dose rate of 0.03 Gy/ka.
6. Mean ± standard error. The error term includes a 2% systematic uncertainty associated with laboratory beta-source calibration. D_e values were calculated using the central age model and minimum age model of Galbraith *et al*. (1999). Those D_e determined using the minimum age model are denoted with (#), and using the three -parameter model, with relative error of 20 % added in quadrature to each single-grain D_e measurement errors prior to running the model; this value represents an

estimate of the minimum amount of overdispersion present in a well-bleached sample of quartz.

7. D_e overdispersion. The spread in D_e values remaining after taking all measurement uncertainties into account.
8. Mean ± total (1σ) uncertainty, calculated as the quadratic sum of the random and systematic uncertainties.

Table 3. Radiocarbon age determinations of charcoal collected from KYC, originally presented in Bronk-Ramsey *et al.*(2015).

Oxford sample laboratory code	Sample type	Sample location	$\delta^{13}C$ (‰)	Radiocarbon age (cal BP)
OxA-23686	Charcoal, *?Eucalyptus*	South pit , Quadrat B, Unit 7	-25.5	1141 ± 25
OxA-23687	Charcoal, *?Eucalyptus*	South pit, Quadrat C, Unit 7	-27.7	904 ± 25
OxA-23688	Charcoal, *?Eucalyptus*	South pit, Quadrat C, adjacent to *Macropus fuliginosus* skeleton, Unit 7	-7.0	1258 ± 26
OxA-23689	Charcoal, *?Eucalyptus*	South pit, Qadrat D, Unit 7, light brown sand beneath flowstone	-4.9	989 ± 25
OxA-23792	Charcoal, *?Eucalyptus*	North pit, Quadrat B, Unit 6, sample B.	-23.3	4566 ± 32

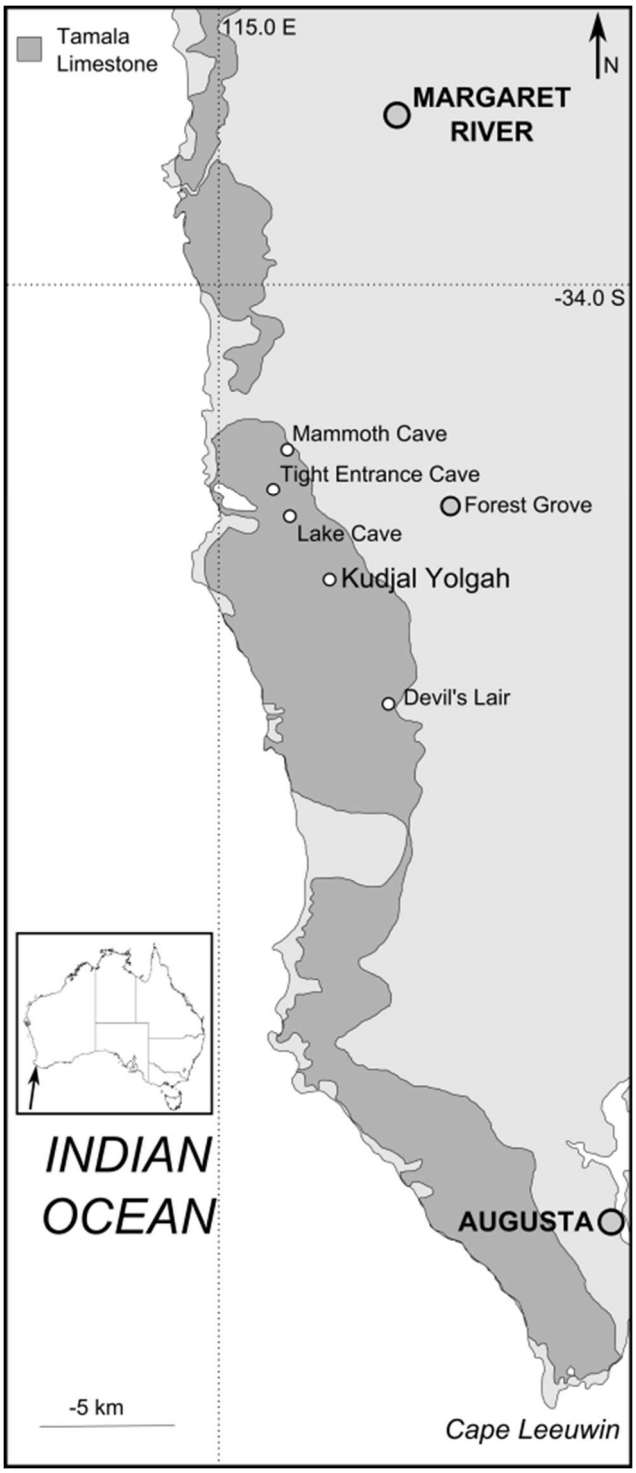

Figure 1. Location of Kudjal Yolgah Cave (Cave Number 6WI-9) in relation to other key sites found in the Tamala Limestone. Inset map shows the location of the Kudjal Yolgah with respect to the Australian continent.

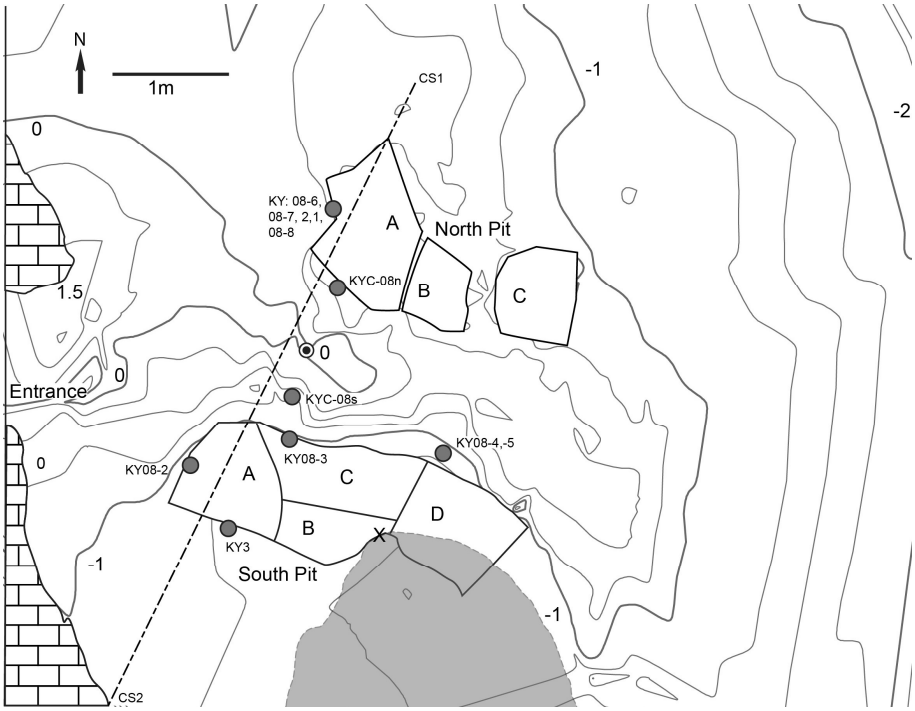

Figure 2. Plan view of KYC excavation area showing the North and South Pits and OSL sample locations. The dashed line (A-A') marks the transect for the cross-sectional profile presented in Figure 3. Light grey represents the initial extent of the south flowstone, dark grey the remaining flowstone. X marks flowstone sample used for U-Th dating. Dense hatch is Unit 2. Eastern dotted contours extrapolated.

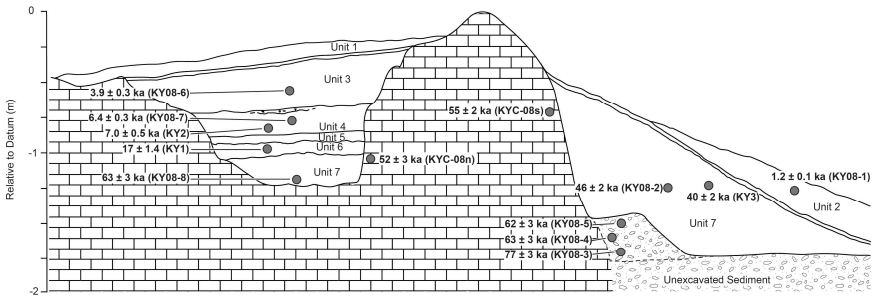

Figure 3. Cross section (A-A', see Fig. 2.) through the North (left) and South (right) Pits. Also shown are the OSL positions, elevations and OSL age estimates. Bird feet hatching represents prior anthropogenic disturbance. Brick symbol equates to limestone boulders and some sediment. Thin light grey layer capping south Unit 7 is flowstone. Dashed pits mark 1997 RGR excavations.

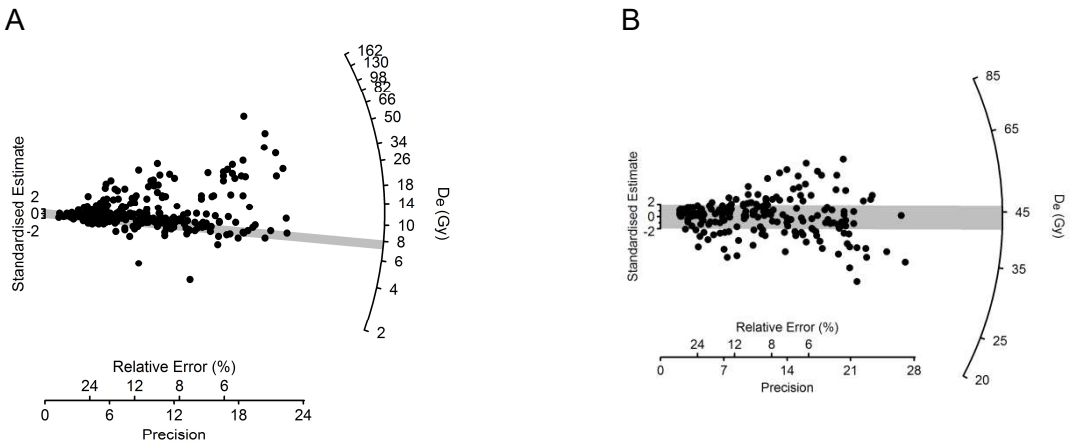

Figure 4.Radial plots showing single-grain D_e distributions from Kudjal Yolgah Cave containing a population of partially-bleached (A: KY08-6) and well-bleached (B: KY3) grains of quartz.

1 OSL methods and supplementary information

1.1 Sample preparation and measurement

In the laboratory, samples were prepared under dim red, light-safe conditions using standard laboratory procedures (Wintle 1997). Samples were washed in 10% HCl acid and 30% H_2O_2 to remove carbonates and organic residues, respectively, and sieved to obtain the 180–212 μm in diameter grain-size fraction. This grain size fraction was density separated using sodium polytungstate to remove the heavy mineral and feldspar grains. The separated quartz grains were then etched in 45% hydrofluoric acid for 40 min to remove the alpha-dosed rinds and any residual feldspar grains (as the HF-acid preferentially targets the feldspar grains). The sample was then sieved again to remove the now much smaller feldspar grains and obtain a 'purified' subsample of 180–212 μm in diameter quartz grains.

The OSL measurements were carried out using an automated Risø TL/OSL reader fitted with a single-grain laser attachment. Laboratory irradiations for all samples were carried out using a calibrated $^{90}Sr/^{90}Y$ beta source delivering ~6 Gy/min. Optical stimulation was achieved using 532 nm (green) light from a 10 mW Nd:YVO4 solid-state diode-pumped laser, focused on to a spot ~20 μm in diameter, at a power density of ~50 W/cm^2 (Bøtter-Jensen *et al.* 2000; Bøtter-Jensen *et al.* 2003). The induced ultraviolet emissions were then detected by an Electron Tubes Ltd 9635Q photomultiplier tube fitted with a pair of U-340 filters.

1.1.1 Dose recovery test

To test the appropriateness of the SAR procedure (Table S1), the preheating conditions used and the adequacy of the data analysis procedures, a single-grain dose-recovery test was performed (Murray & Roberts, 1997) on one sample from KYC (KY08-5). A small subsample of HF-etched 180–212 μm quartz grains were bleached by natural sunlight for several days and then given a laboratory beta dose of 70 Gy; this dose is close to the expected burial dose for most of the samples and represents a 'surrogate natural' dose.

The resultant dose distribution is shown as a radial plot in Fig. S1. The recovered dose values are distributed symmetrically around a central value of 69.4 ± 0.6 Gy, estimated using the Central Age Model (CAM) of Galbraith *et al.* (1999), and is consistent with the 70 Gy applied laboratory beta dose. This result indicates that the measurement and analytical procedures employed can recover the correct (known) dose for the samples from this region under controlled laboratory conditions. It should be noted, however, that the measured doses are spread more widely than can be accounted for solely on the basis of their measurement uncertainties, with an 'overdispersion' (OD) value of 6.4 ± 0.9%. This finding is in keeping with numerous single-grain quartz dose recovery tests, with this value similar to those reported for other single-grain dose recovery tests (Roberts *et al.* 2000; Jacobs *et al.* 2003b; Thomsen *et al.* 2005, 2012; Jankowski *et al.* 2014). Passing the dose-recovery test is a minimum requirement for reliable application of the SAR procedure (Roberts *et al.* 1999).

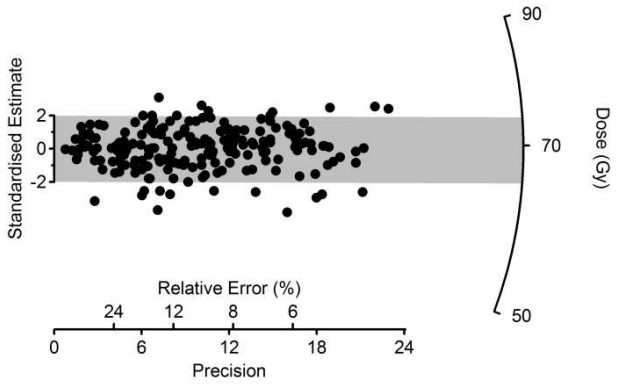

Fig. S1. Radial plot for single grains of quartz from sample KY08-5 (n = 193) that had been bleached and then given a dose of 70 Gy before measurement using the SAR procedure of Table S1. This dose recovery test was performed to assess the suitability of the experimental conditions used to measure the absorbed dose. The grey band on the radial plot should capture 95% of the points if the measured doses are consistent with the given dose at 2σ. In this case, the points are slightly overdispersed (OD = 6.4 ± 0.9%), as is typical for quartz.

1.2 Equivalent dose (D_e) determination measurement and analysis procedures

The D_e of the individual grains was measured using the single-aliquot regenerative-dose (SAR) procedure (Murray & Roberts 1998; Murray & Wintle 2000, 2003). The procedure used in this study is outlined in Table S1. Prior to the OSL measurement of the natural or regenerative doses, the sample was heated to 240 ˚C for 10 s (Step 1). The OSL for each individual grain was then measured using the green laser set at a constant power of 45 W/cm^2 for 2 s to produce a decay curve of OSL intensity with stimulation time (Step 2). The first and last 0.1 s of data represent the instrumental counts collected with the laser switched off. During optical stimulation the sample was held at 125 ˚C to ensure that charge was not re-trapped in the 110 ˚C TL peak (Wintle & Murray 1997). A test dose was given after measurement of the natural and each regenerative dose (Step 3). The sample was then preheated to 160 ˚C for 5 s (Step 4) before the OSL signal was, once again, measured using the green laser and holding the sample at 125 ˚C (Step 5; as per Step 2). The test dose induced OSL signal was used to monitor and correct for any changes in sensitivity that occurred over the SAR cycles.

The OSL signal for each dose point was estimated from the first 0.2 s of OSL decay to target the 'fast' OSL component, with a background count subtracted. The latter was determined from the mean count rate over the last 0.3 s of laser stimulation. By standardising the natural and regenerative dose OSL signals against their respective test dose OSL signals, a sensitivity-corrected OSL signal is found from which a sensitivity-corrected dose-response curve can be generated.

Table S1. SAR procedure used throughout this study for dose recovery experiments and the determination of D_e values for naturally-irradiated quartz grains.

Step	Treatment	Purpose
1	Preheat (PH1) to 240 ˚C for 10 s	–
2	Stimulate using focussed green laser for 2 s at 125 ˚C	Induce OSL from natural or regenerative dose
3	Test dose	–
4	Preheat (PH2) to 160 ˚C for 5 s	–
5	Stimulate using focussed green laser for 2 s at 125 ˚C	Induce OSL from test dose
6	Regenerative dose	–
7	Return to step 1 and repeat at least 3 times altering the size of the regenerative dose	–
8	Give 0 Gy dose and repeat steps 1–5	Check for recuperation (Rejection criterion 5)
9	Repeat first regenerative dose and steps 1–5	Check recycling ratio (Rejection criterion 2)
10	Repeat first regenerative point	–
11	Stimulate using infrared diodes for 40 s at 50 ˚C	–
12	Repeat steps 1–5	Check for feldspar contamination (Rejection criterion 3)

It is well known that there is large variability in the OSL behaviours of individual grains from the same sample and that the SAR measurement conditions employed are not always appropriate for every grain (Murray & Roberts 1997; Murray *et al.* 1997; Roberts *et al.* 1999; Duller & Murray 2000; Thomsen *et al.* 2005; Jacobs *et al.* 2012; Gliganic *et al.* 2012a; Medialdea *et al.* 2014). To overcome this problem, each measured grain was assessed against a set of formal criteria, based on those described by Jacobs et al. (2006a; 2006c). Grains were rejected if:

1) the OSL signal induced by the test dose given immediately after measurement of the natural OSL signal was less than 3 times the respective background count;
2) the 'recycling ratio' (the ratio of the sensitivity-corrected OSL signals produced by 2 identical regenerative doses) differed from unity by more than 2σ;

3) the OSL-IR depletion ratio of Duller (2003) (to check for feldspar contamination) was smaller than unity by more than 2σ;
4) the sensitivity-corrected OSL signal measured after preheating a 0 Gy regenerative dose (used to check for thermal transfer) was greater than 5% of the sensitivity-corrected natural OSL signal;
5) the sensitivity-corrected natural OSL signal failed to intercept the dose-response curve.

For grains that were not removed during the screening procedure above, D_e values were calculated by fitting a dose-response curve to the sensitivity-corrected regenerative dose points and projecting the sensitivity-corrected natural OSL signal on to this curve to obtain the D_e by interpolation. Curves were fitted using either a single saturating exponential function or one with an extra linear term. The total uncertainty on the D_e includes allowance for photon counting statistics (Galbraith 2002; Galbraith *et al.* 2005), instrumental reproducibility (Jacobs *et al.* 2006c), and errors in curve fitting estimated by Monte Carlo simulation using Analyst version 3.24 (Duller 2007).

Of the 10 900 grains measured, 4 025 were accepted, equating to 37% usable grains. A full breakdown of the rejection criteria and the causes for their rejection are shown in Table S2. The D_e values of accepted grains are considered meaningful in terms of burial dose. The majority of grains accepted were intensely luminescent and dominated by a 'fast' OSL component, which decayed rapidly in the first 0.2 s of laser stimulation, although some take up to 0.5 s to reach a stable background. Fig. S2 shows 10 representative decay curves for KY2 (Unit 4), KY1 (Unit 6) and KYC-08n (Unit 7). The majority of the grains produced well-behaved dose-response curves that could be fitted with either a single saturating exponential or a saturating exponential plus an additional linear term (Fig. S3).

The D_e values and associated uncertainties were then displayed as radial plots (Galbraith 1998, 2010; Galbraith & Roberts 2012), to visually assess the D_e distributions of the samples. The radial plots for each of the 14 samples examined in this study are shown in Fig. S4. Using D_e distribution patterns, as well as independent age control and an understanding of the processes of site formation, either the minimum (MAM) or the central age model (CAM) of Galbraith *et al.* (1999) were used to statistically determine the D_e of each sample. These results are shown in Table 1 in the main text.

Table S2. Breakdown of the number of grains measured, rejected and accepted according to the rejection criteria outlined in section 1.2.

Sample name	No. of grains measured	Grain rejected because of failure to meet criteria:					Total grains rejected	Total grains accepted	Return (%)
		1	2	3	4	5			
KY1	500	254	24	19	13	12	322	178	36
KY2	500	209	57	32	13	14	325	175	35
KY3	500	205	41	19	9	21	295	205	41
KY08-1	900	370	105	32	299	30	836	64	7
KY08-2	900	310	77	21	15	55	478	422	47
KY08-3	900	298	110	23	15	66	512	388	43
KY08-4	800	345	57	16	7	82	507	293	37
KY08-5	900	328	134	23	9	52	546	354	39
KY08-6	900	412	145	53	19	4	633	267	30
KY08-7	900	379	111	20	17	13	540	360	40
KY08-8	900	334	120	35	9	41	539	361	40
KY08-9	1000	412	144	27	15	18	616	384	38
KYC-08n	400	120	102	8	7	19	256	144	36
KYC-08s	900	253	78	18	28	93	470	430	48
Total	10900	4229	1305	346	475	520	6875	4025	**Mean = 37**

Rejection criteria numbers are as follows:

1) the OSL signal induced by the test dose given immediately after measurement of the natural OSL signal was less than 3 times the respective background count;
2) the 'recycling ratio' (the ratio of the sensitivity-corrected OSL signals produced by 2 identical regenerative doses) differed from unity by more than 2σ;
3) the OSL-IR depletion ratio of Duller (2003) (to check for feldspar contamination) was smaller than unity by more than 2σ.
4) the sensitivity-corrected OSL signal measured after preheating a 0 Gy regenerative dose (used to check for thermal transfer) was greater than 5% of the sensitivity-corrected natural OSL signal;
5) the sensitivity-corrected natural OSL signal failed to intercept the dose-response curve.

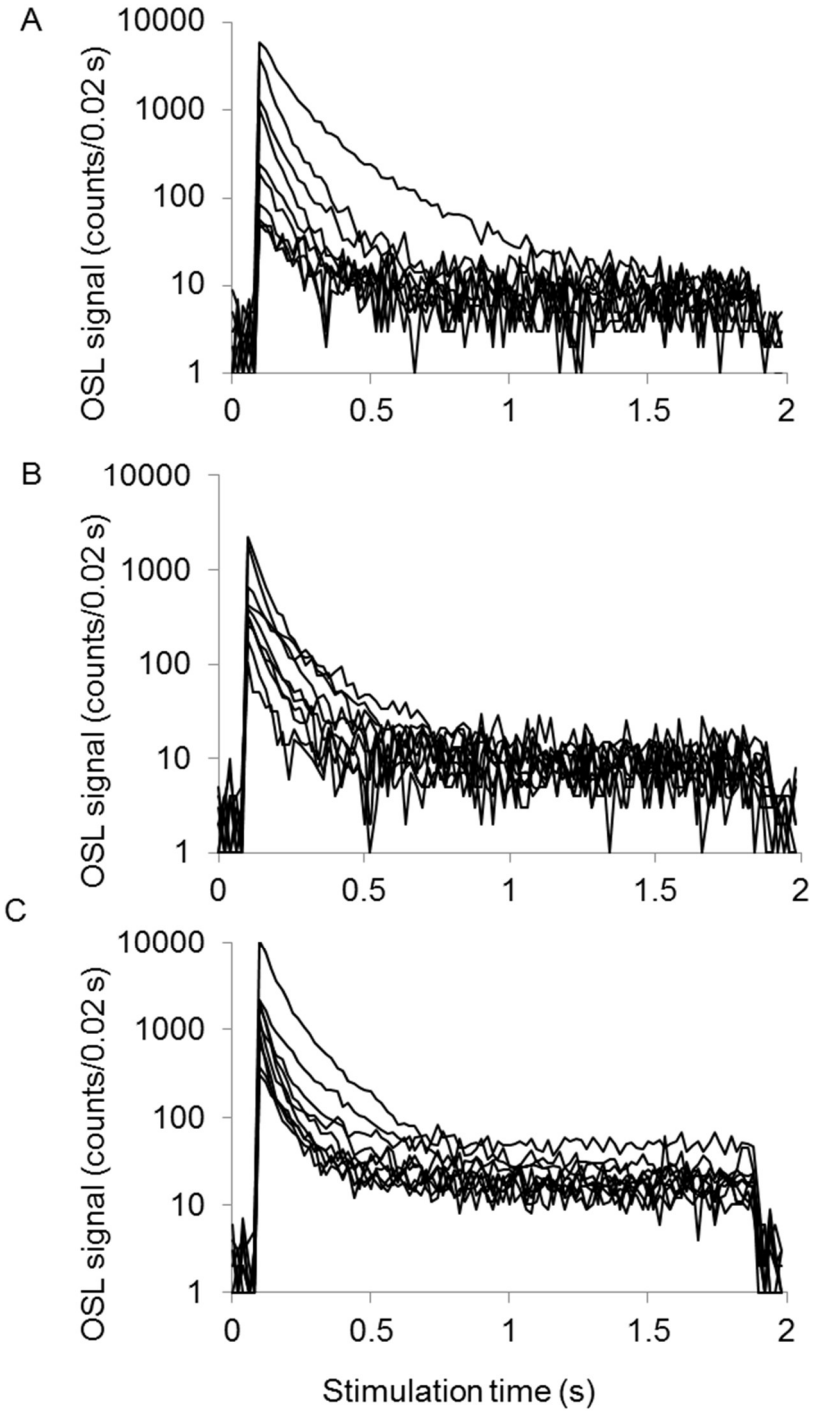

Fig. S2. OSL decay curves for samples: A) KY2, B) KY1, and C) KYC-08n for ten accepted grains showing the range of variability in the decay characteristics within samples and KYC. In the majority of cases the initial signals decaying quite rapidly to a stable background (between 0.2 and 0.5 s).

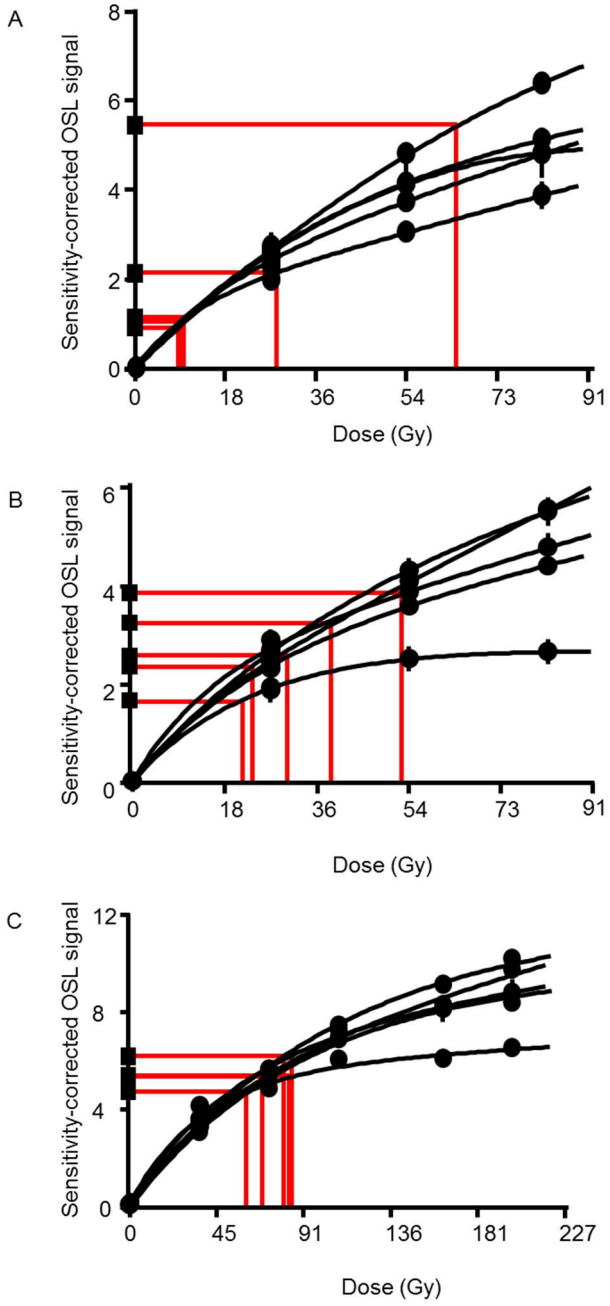

Fig. S3. Dose-response curves for five single grain of quartz from samples: a) KY2, b) KY1, and c) KYC-08n.

A

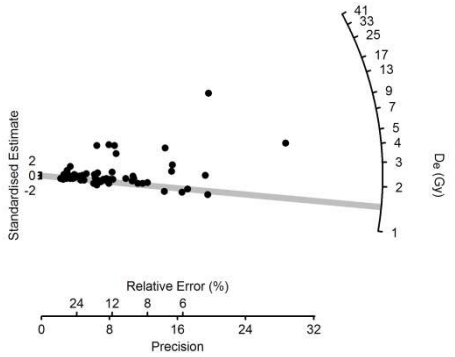
Standardised Estimate
2
0
-2
De (Gy)
41
33
25
17
13
9
7
5
4
3
2
1
Relative Error (%)
24 12 8 6
0 8 16 24 32
Precision

B

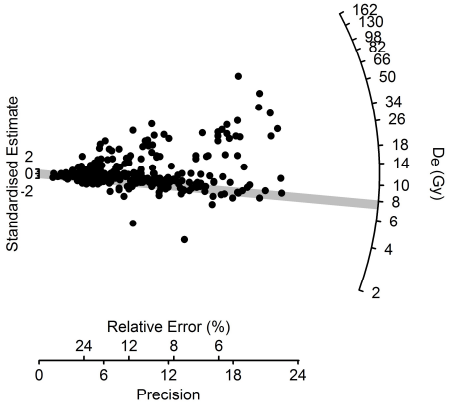
Standardised Estimate
2
0
-2
De (Gy)
162
130
98
82
66
50
34
26
18
14
10
8
6
4
2
Relative Error (%)
24 12 8 6
0 6 12 18 24
Precision

C

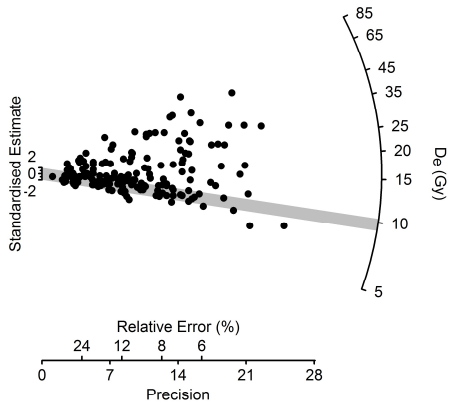
Standardised Estimate
2
0
-2
De (Gy)
85
65
45
35
25
20
15
10
5
Relative Error (%)
24 12 8 6
0 7 14 21 28
Precision

D

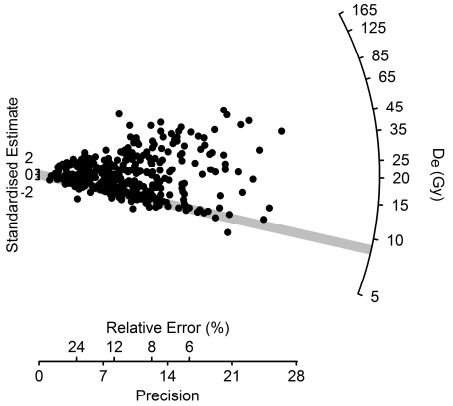
Standardised Estimate
2
0
-2
De (Gy)
165
125
85
65
45
35
25
20
15
10
5
Relative Error (%)
24 12 8 6
0 7 14 21 28
Precision

E

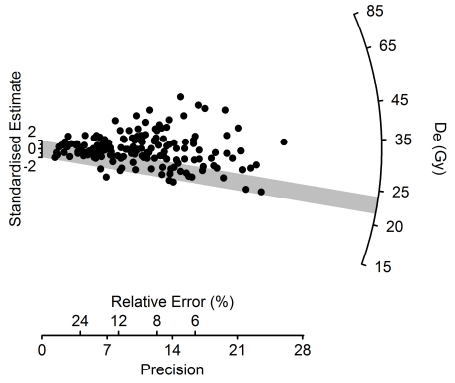
Standardised Estimate
2
0
-2
De (Gy)
85
65
45
35
25
20
15
Relative Error (%)
24 12 8 6
0 7 14 21 28
Precision

F

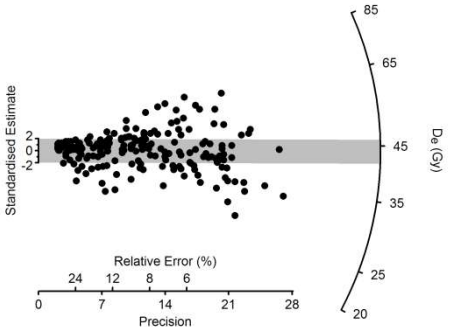
Standardised Estimate
2
0
-2
De (Gy)
85
65
45
35
25
20
Relative Error (%)
24 12 8 6
0 7 14 21 28
Precision

G

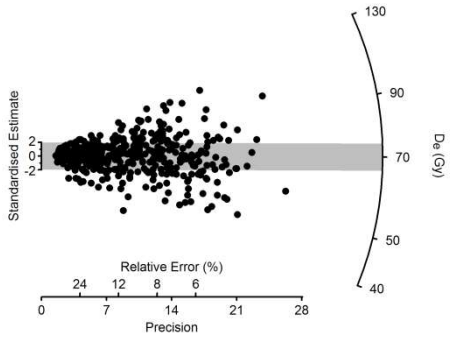
Standardised Estimate
2
0
-2
Relative Error (%)
24
12
8
6
0
7
14
21
28
Precision
130
90
70
50
40
De (Gy)

H

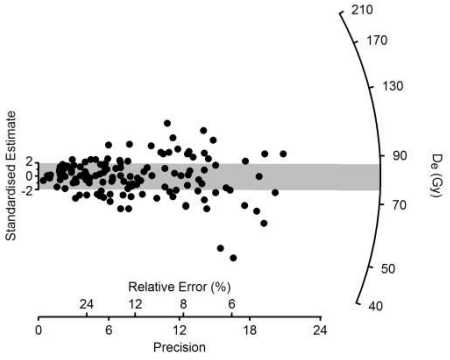
Standardised Estimate
2
0
-2
Relative Error (%)
24
12
8
6
0
6
12
18
24
Precision
210
170
130
90
70
50
40
De (Gy)

I

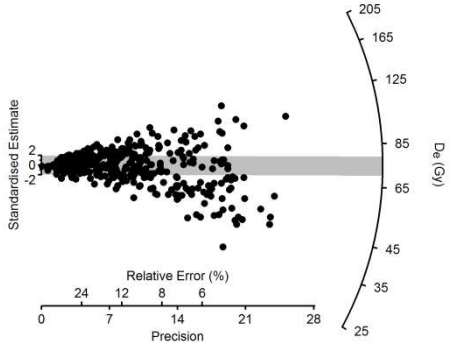
Standardised Estimate
2
0
-2
Relative Error (%)
24
12
8
6
0
7
14
21
28
Precision
205
165
125
85
65
45
35
25
De (Gy)

J

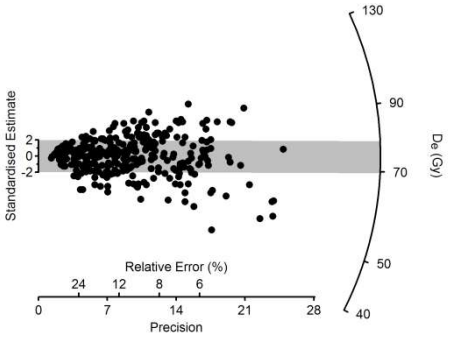
Standardised Estimate
2
0
-2
Relative Error (%)
24
12
8
6
0
7
14
21
28
Precision
130
90
70
50
40
De (Gy)

K

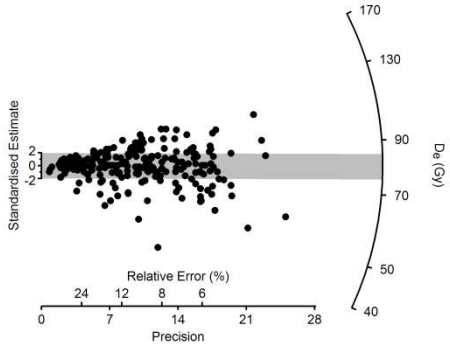
Standardised Estimate
2
0
-2
Relative Error (%)
24
12
8
6
0
7
14
21
28
Precision
170
130
90
70
50
40
De (Gy)

L

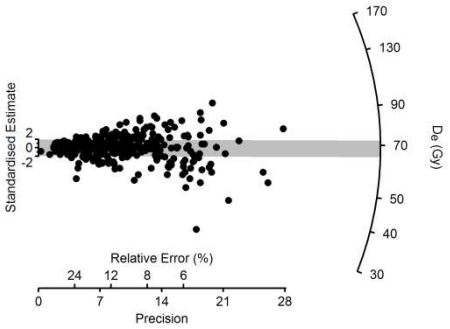
Standardised Estimate
2
0
-2
Relative Error (%)
24
12
8
6
0
7
14
21
28
Precision
170
130
90
70
50
40
30
De (Gy)

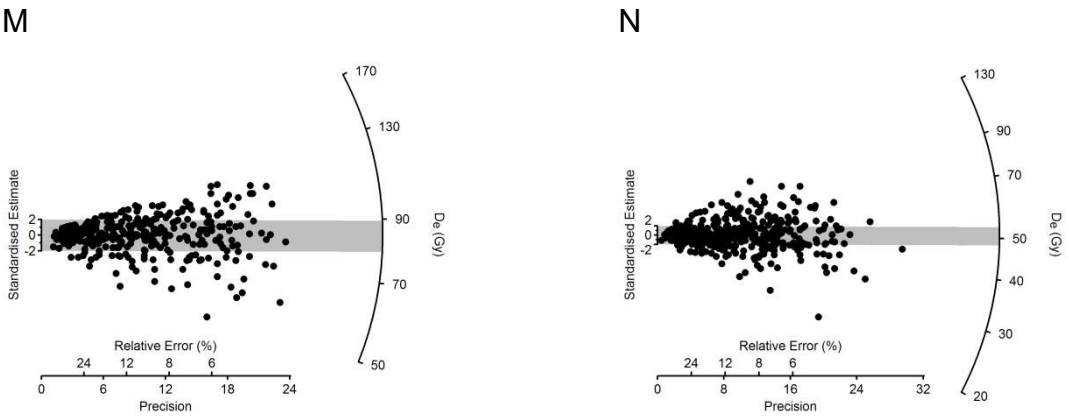

Fig. S4. Radial plots showing single-grain D_e distributions for: A) KY08-1; B) KY08-6; C) KY2; D) KY08-7; E) KY1; F) KY3; G) KY08-2; H) KYC-08n; I) KYC-08s; J) KY08-5; K) KY08-4; L) KY08-8; M) KY08-3; N) KY08-9.

1.3 Dose rate (D_r) determination

The effective D_r to the hydrofluoric acid-etched quartz grains is derived from gamma rays, beta particles, internal alpha particles and cosmic rays. The fact that the investigated samples were collected over a decade and by three separate 'teams' means that the methods used for D_r determination are different due to the available equipment and 'expertise' of the sampling team. In addition, constraining sedimentary features, such as buried flowstones and limestone éboulis, rendered the application of *in situ* gamma D_r determination inappropriate in some instances. Table S3 outlines which methods were used for each sample with regards to beta and gamma D_r determination. The internal alpha and cosmic D_r assumed and estimated based on published data and formulae, respectively.

With respect to the beta and gamma D_r, emission counting methods were used. These methods included: Geiger-Müller beta counting (GMBC; Bøtter-Jensen & Mejdahl 1988); thick-source alpha counting (TSAC; Aitken 1985); *in situ* gamma detector measurement (Løvborg & Kirkegaard 1974; Murray *et al.* 1978; Murray *et al.* 1987) and; high resolution gamma spectrometry (Murray *et al.* 1987). By using emission counting methods it was assumed that the current state of (dis)equilibrium in the ^{238}U and ^{232}Th decay chains has been present over the duration of the burial period.

Table S3. Table outlining the methods used in the determination of the environmental dose rates, where GMBC is Geiger Muller beta counting, HRGS is high resolution gamma spectrometry, and TSAC is thick-source alpha-counting.

Sample	Beta dose rate determination method		Gamma dose rate determination method		
	GMBC	HRGS	2-inch gamma detector	3-inch gamma detector	TSAC+GMBC
KY08-1	X		X		
KY08-6	X		X		
KY2	X	X		X	
KY08-7	X		X		
KY1	X	X		X	
KY3	X	X		X	
KY08-2	X				X
KY-08n	X				X
KY-08s	X				X
KY08-5	X		X		
KY08-4	X		X		
KY08-8	X		X		
KY08-3	X		X		
KY08-9	X		X		

1.3.1 Sample preparation

With the exception of *in situ* gamma detector measurements, each of the remaining methods requires that additional sediment samples be collected. These samples were either collected from the back of the OSL sampling holes (all KY08 and KY samples) or from the light exposed ends of the OSL sampling tubes (both KYC-08 samples). Each sample was weighed, oven dried and weighed again to obtain a measure of current sediment moisture content (see section 1.3.7). The dried samples were then pulverised and homogenised to produce a fine powder that would be used in laboratory determination of both beta and gamma D_r values. Using laboratory-based techniques implicitly assumes that the samples being measured are representative of homogeneous spheres of beta or gamma radiation, although such assumptions are known to be unrealistic in natural sediments (Murray *et al.* 1997; Nathan *et al.* 2003; Guérin *et al.* 2012b)

1.3.2 Beta D_r determination

1.3.2.1 GMBC

Beta D_r were measured directly using a GM-25-5 multi-counter system (Bøtter-Jensen & Mejdahl 1988) for all 14 samples (all KY08 and KYC-08: Table S3). The samples were loaded into individual sample holders or 'pots,' measuring 25 mm in diameter and 6 mm in depth, and measured simultaneously for a period of 24 hr. The uncertainty on the beta D_r was calculated using the method described in Jacobs & Roberts (2015).

1.3.2.2 HRGS

Unlike the previously discussed methods of emission counting, HRGS not only provides an estimate of the beta D_r coming from U, Th and K, but also has the ability to determine the presence, and the extent of, any disequilibrium in either the ^{238}U or ^{232}Th chains. The HRGS measurements were made by Roberts *et al.* (2001) at CSIRO Water, Canberra, Australia in March 1999 on resin-pressed pulverised samples of KY1, KY2 and KY3 collected during 1997. We present the results of the Roberts *et al.* (2001) HRGS measurements here in Table S4. These results were then converted into beta D_r using the conversion factors of Guérin *et al.* (2011) and the analytical uncertainties propagated appropriately.

Table S4. Radionuclide activities for selected samples from Kudjal Yolgah Caves determined using high-resolution gamma-ray spectrometry.

Sample code	Unit	Radionuclide Activities (Bq/kg)					
		^{238}U	^{226}Ra	^{210}Pb	^{228}Ra	^{228}Th	^{40}K
KY1	6	8.9 ± 1.4	12.1 ± 0.2	12.8 ± 1.6	33.8 ± 0.6	33.2 ± 0.4	197.3 ± 4.1
KY2	4	11.9 ± 2.4	13.3 ± 0.4	7.0 ± 2.7	34.9 ± 1.0	34.1 ± 0.7	188.5 ± 6.8
KY3	7	8.1 ± 1.9	9.7 ± 0.3	7.5 ± 1.8	25.6 ± 0.9	24.2 ± 0.5	159.7 ± 5.8

1.3.3 Beta D_r attenuation

All beta D_r were adjusted for grains size and moisture content (Aitken 1985; Brennan 2003). The amount of attenuation experienced by a beta particle is dependent upon the radionuclide it is being released from and the size of the grain it is penetrating. All beta D_r were adjusted to account for the attenuation and the influence of HF-acid etching using the values presented in Brennan (2003). Furthermore a systematic 3% error is added in quadrature to the random beta D_r uncertainty to account for systematic uncertainty in the attenuation factors.

1.3.4 Gamma D_r determination

1.3.4.1 TSAC and GMBC

The TSAC and GMBC method for determining the gamma D_r was used for 3 samples; KYC-08n, KYC-08s and KY08-2. For both KYC samples, collected by GJP and GG, the sediments from which these samples were taken was excavated during the January 2008 field season and therefore not available for *in situ* gamma detector measurements in the following October by NRJ, RGR and ZJ. *In situ* gamma detector measurements could not be made for sample KY08-2 during the October season as a large limestone block prevented the complete insertion of the gamma detector into the OSL hole.

As a standalone technique, TSAC provides an estimate of the beta and gamma D_r contributions coming from U and Th only (Aitken 1985, 1990). However, when used in combination with an independent measurement for K (e.g., GMBC as was used here), the total gamma D_r can be determined. The alpha D_r was determined using the 'pairs' counting technique of Aitken (1990) and Daybreak 583 thick-source alpha counter. As GMBC was carried out alongside TSAC, the concentrations of U, Th (from the TSAC) and also K (from the TSAC and beta counting) were calculated using the equations and methods outlined in Appendix J in Aitken (1985) and converted into D_r (Gy/ka) using the conversion factors of Guérin *et al* .(2011).

1.3.4.2 2-inch in situ gamma detector measurements

The external gamma D_r is most accurately determined using a field gamma detector (FGD) at the time of sampling. This technique, unlike the HRGS, or TSAC and GMBC, takes into account the heterogeneity of the surrounding gamma sphere with respect to the sample position (Murray *et al.* 1978; Murray 1981; Murray *et al.* 1987). The total gamma flux emitted from the sediments is an admixture coming from ^{238}U, ^{232}Th (and their radioactive progeny) and ^{40}K. Here, the measured gamma emission spectrum are used to ascertain the contribution of each of these radionuclides to the total gamma D_r.

The 2-inch FGD was used to determine the gamma D_r contribution for 10 of the 11 KY08 samples (Table S3). The 2-inch FGD was calibrated by Z. Jacobs using the 'Oxford Blocks' (Rhodes & Schwenninger 2007) located at the Research Laboratory for Archaeology and History of Art, Oxford University. The measurement of the gamma D_r was conducted by first enlarging the sample hole to the appropriate size to allow the detectors to be fully inserted

into the sediment. The gamma spectrum at each measurement position was measured for a duration of between 30 min and 1 hr. The total gamma D_r was determined using the threshold technique (Løvborg & Kirkegaard 1974; Murray *et al.* 1978; Aitken 1985; Mercier & Falguères 2007). A relative uncertainty of 5% was applied to each 2-inch gamma detector measurement throughout this study. This estimate of uncertainty is based upon: 1) counting statistics, 2) instrument drift, 3) instrument reproducibility, and 4) uncertainty in the calibration brick housing used at the University of Wollongong.

1.3.4.3 3-inch gamma detector measurements

A 3-inch GR-320 Exploranium NaI(Tl) FGD was used to determine the gamma D_r for the 3 KY samples collected during 1997 by Roberts *et al.* (2001)(Table S3). Here, we converted the concentrations of U, Th and K into into D_r (Gy/ka) using the D_r conversion factors of Guérin *et al.* (2011). The mean gamma D_r for U, Th and K (and their associated standard errors) were calculated separately and then summed to provide an estimate of the total environmental gamma D_r. The uncertainty on the total gamma D_r was taken as the quadratic sum of the standard errors.

1.3.5 Cosmic D_r determination

The cosmic D_r for all samples was estimated using the published relationships presented in Prescott & Hutton (1994). Here a latitude of -34.0º S and longitude of 115.0º E were used along with an altitude of 50 m. A constant rock overburden of 5 m was accounted for in each calculation with an assumed density of 1.2 g/cm^3, as well as the depth of the sedimentary over of each sample where a density of 2.0 g/cm^3 was assumed. An uncertainty of ±10% was assumed for all estimates.

1.3.6 Internal alpha D_r determination

An internal alpha dose ate of 0.03 ± 0.01 Gy/ka was assumed for all samples.

1.3.7 Moisture content

It is also important that the fluctuations in the sediment moisture content over the period of burial be accounted for (Aitken 1985, Aitken & Xie 1990, Aitken 1998). The sediment moisture content (either held in pores or bound in clay) absorbs a proportion of the incoming radiation. As a general rule, a ~1% increase in sediment moisture content decreases the total environmental D_r by ~1%; producing an increase in OSL age by ~1% (Lian & Roberts 2006; Jacobs & Roberts 2007). Thus, the beta, gamma and cosmic D_r which are measured or estimated as 'dry' (with the exception of *in situ* gamma detector measurements) are required to be corrected for moisture content absorption.

An estimate of sediment moisture content was made by collecting a portion of sediment at the time of sampling for all samples except those labelled KYC-08. For these samples the light exposed ends of the OSL sample plastic tubes was used. The samples were weighed before

and after a period of oven drying. The difference between these two measurements is expressed as a percentage of the dried sample mass. At KYC, the current moisture contents range between 1.4 and 5.2%. These values were used to 'dry' all the *in situ* gamma detector measurements which were made at field moisture content at the time of sampling.

A sediment moisture content of 5 ± 2 (1σ) was assumed as representative for all samples collected from KYC as this value encompassed a broad range that covers the extent of all measured values made in this study (Table 1 in the main text). We consider that this value is appropriate for these samples, with regards to the historical fluctuations in moisture content, for two reasons. First, the sediments are dominated by sand 125–750 μm with little silt or clay (see supplementary information section 2 and Table S6) resulting in a clast-supported sediment. Such sediments are known to have both high porosity and permeability values. Second, the lack of any significant amount of clay in the sediments means that no significant amount of water would be held within the clay mineral lattice. The ultimate outcome of these sedimentological characteristics is that any water percolating through the sediment would be able to move freely, and relatively quickly, through the pore space network. The moisture content correction coefficient were calculated using the equations found in Aitken (1985) and Nathan & Mauz (2008).

The total environmental D_r for each sample (as presented in Table 1 of the main text) is the sum of the moisture-corrected external cosmic, gamma and (attenuated) beta D_r and the internal alpha D_r.

1.3.8 Dose rate determination comparison

Given that a number of different methods were used in the evaluation of both the beta and gamma dose rates, a comparison of the impact that these measurements have on the resulting OSL ages were warranted. Table S5 provides the results of this comparison. For the three samples investigated, the HRGS gamma dose rate was significantly larger than the FGD. This finding, however, is not unexpected. HRGS analysis only provides an estimate of the gamma dose rate coming from the subsample of sediments collected for analysis and does not take into account any heterogeneity within the gamma sphere of influence for the given samples. Given the complex nature of the KYC deposit, clastic sands interspersed with numerous limestone pebbles and cobbles, calcite precipitates and laminated, bifurcating flowstones, it is unlikely that the concept of infinite matrix hold true at KYC. We prefer, therefore, to use the *in situ* gamma detector measurements for the determination of the gamma dose rate for our samples.

The ratio of the beta dose rates determined using the HRGS and GMBC, for all but one sample (KY1) are consistent with unity. To check the sensitivity of the ages to the use of either the HRGS or GMBC beta dose, a ratio of the OSL ages using these two methods was taken. Here, the gamma dose rate for both samples were those determined using the *in situ* gamma detectors, whereas the beta dose rate used was determined using the HRGS or GMBC determination (Table S5). The ratios show that the OSL ages are relatively insensitive to which of these two methods is used; for KY2 and KY3 the ages are consistent with unity at

1σ, and KY1 at 2σ. To maintain consistency throughout our data set, the GMBC beta dose rate was used in the age determination of all samples.

Table S5. Comparison of the gamma and beta dose rate determination methods and their impact of the subsequent OSL ages.

	Gamma[1]	Beta[2]	Age ratio[3]	Age ratio[4]
	HRGS/FGD	HRGS/Beta	FGD+HRGS/FGD+GMBC	HRGS/FGD+GMBC
KY1	1.72 ± 0.09	1.30 ± 0.08	0.87 ± 0.07	0.72 ± 0.06
KY2	1.37 ± 0.09	1.07 ± 0.08	1.02 ± 0.09	0.90 ± 0.08
KY3	1.15 ± 0.07	0.98 ± 0.07	0.97 ± 0.07	0.92 ± 0.07

1. Gamma dose rates determined using either high resolution gamma spectrometry (HRGS) or *in situ* field gamma detector (FGD)
2. Beta dose rates determined using either high resolution gamma spectrometry (HRGS) or Geiger Muller Beta Counter (GMBC)
3. Numerator ages calculated using FGD for gamma dose rate and HRGS for beta dose rate. Denominator ages calculated using FGD for gamma dose rate and GMBC for beta dose rate.
4. Numerator ages calculated using HRGS for both the gamma and beta dose rates. Denominator ages calculated using FGD for gamma dose rate and GMBC for beta dose rate.

2 Sedimentology

A small subsample of each of the KYC OSL samples was removed for a basic sediment analysis. Approximately 15 g of sediment was examined for colour using a Munsell Soil Color Chart (1994) on dry samples and angularity under a dissecting microscope.

Sediment grain size analysis was conducted using a Malvern Mastersizer 2000. The carbonate cement was removed using a 5% hydrochloric acid solution, which was decanted after 5 days to allow the clay to settle. The sample was then washed with demineralised water to remove any precipitate salts and decanted using the same process. Prior to measurement, the sediments were mixed into a thick slurry to ensure large grain sizes were not preferentially sampled. Each sample was measured at a fan speed of 3750 rpm and a laser obscuration of 7–10%. The results of the ten sample analysed in this study are presented in Table S6.

Table S6. Basic sedimentological data, including grain size distribution, Munsell colour, angularity, and sedimentological descriptions following those of Folk & Ward (1957) for the OSL samples collected over the 2007-2008 field seasons

Sample Name	Unit	Grain size cumulative proportions (μm)									Munsell colour	Angularity	Folk and Ward (1957) descriptions			
		0.2	3.9	62.5	125	250	500	750	1000	2000			Mean	Sorting	Skewness	Kurtosis
KY08-1	2	0	1	12	17	25	45	68	86	100	10YR 4/2	Rounded	Coarse Sand	Moderately Sorted	Very Fine Skewed	Very Platykurtic
KY08-6	3	0	2	10	14	28	58	80	93	100	7.5YR 4/4	Rounded	Coarse Sand	Moderately Sorted	Very Fine Skewed	Platykurtic
KY08-7	4	0	1	6	9	19	45	67	82	100	7.5YR 5/4	Rounded	Coarse Sand	Moderately Well Sorted	Very Fine Skewed	Platykurtic
KYC-08s	7	0	0	3	6	15	45	71	89	100	7.5YR 4/4	Rounded to sub-rounded	Very Coarse Sand	Moderately Well Sorted	Very Fine Skewed	Very Platykurtic
KYC-08n	7	0	0	4	9	27	59	80	92	100	7.5YR 5/6	Rounded to sub-rounded	Coarse Sand	Moderately Well Sorted	Very Fine Skewed	Very Platykurtic
KY08-2	7	0	0	4	8	25	63	85	96	100	7.5YR 4/4	Rounded to sub-rounded	Coarse Sand	Moderately Well Sorted	Very Fine Skewed	Very Platykurtic
KY08-3	7	0	0	3	6	22	59	82	96	100	7.5 6/6	Rounded to sub-angular	Coarse Sand	Moderately Well Sorted	Very Fine Skewed	Very Platykurtic
KY08-4	7	0	2	8	11	26	61	82	94	100	7.5YR 5/4	Rounded to sub-rounded	Coarse Sand	Moderately Sorted	Very Fine Skewed	Very Platykurtic
KY08-5	7	0	2	11	19	43	77	90	96	100	7.5YR 6/4	Rounded to sub-rounded	Coarse Sand	Moderately Well	Very Fine Skewed	Platykurtic
KY08-8	7	0	0	3	7	24	57	78	92	100	7.5YR 5/6	Rounded	Coarse Sand	Moderately Well Sorted	Very Fine Skewed	Very Platykurtic

References

Aitken, M. J. 1985: *Thermoluminescence dating*. 267 pp. Academic Press, London.

Aitken, M. J. 1990: Pairs precision required in alpha counting. *Ancient TL 8*, 12 - 14.

Bøtter-Jensen, L., Andersen, C. E., Duller, G. A. T. & Murray, A. S. 2003: Developments in radiation, stimulation and observation facilities in luminescence measurements. *Radiation Measurements 37*, 535-541.

Bøtter-Jensen, L., Bulur, E., Duller, G. A. T. & Murray, A. S. 2000: Advances in luminescence instrument systems. *Radiation Measurements 32*, 523-528.

Bøtter-Jensen, L. & Mejdahl, V. 1988: Assessment of beta dose-rate using a GM multicounter system. *International Journal of Radiation Applications and Instrumentation. Part D. Nuclear Tracks and Radiation Measurements 14*, 187-191.

Brennan, B. J. 2003: Beta doses to spherical grains. *Radiation Measurements 37*, 299-303.

Duller, G. A. T. 2003: Distinguishing quartz and feldspar in single grain luminescence measurements. *Radiation Measurements 37*, 161-165.

Duller, G. A. T. 2007: Assessing the error on equivalent dose estimates derived from single aliquot regenerative dose measurements. *Ancient TL 25*, 15-24.

Duller, G. A. T. & Murray, A. S. 2000: Luminescence dating of sediments using individual mineral grains. *Geologos 5*, 87-106.

Folk, R. L. & Ward, W. C. 1957: Brazos River bar: a study in the significance of grain size parameters. *Journal of Sedimentary Petrology 27*, 3-26.

Galbraith, R. 2002: A note on the variance of a background-corrected OSL count. *Ancient TL 20*, 49-51.

Galbraith, R. F. 1998: The trouble with "probability density" plots of fission track ages. *Radiation Measurements 29*, 125-131.

Galbraith, R. F. 2010: On plotting OSL equivalent doses. *Ancient TL 28*, 1-9.

Galbraith, R. F. & Roberts, R. G. 2012: Statistical aspects of equivalent dose and error calculation and display in OSL dating: An overview and some recommendations. *Quaternary Geochronology 11*, 1-27.

Galbraith, R. F., Roberts, R. G. & Yoshida, H. 2005: Error variation in OSL palaeodose estimates from single aliquots of quartz: a factorial experiment. *Radiation Measurements 39*, 289-307.

Gliganic, L. A., Jacobs, Z. & Roberts, R. G. 2012a: Luminescence characteristics and dose distributions for quartz and feldspar grains from Mumba rockshelter, Tanzania. *Archaeological and Anthropological Sciences 4*, 115-135.

Guérin, G., Mercier, N. & Adamiec, G. 2011: Dose-rate conversion factors: update. *Ancient TL 29*, 5-8.

Guérin, G., Mercier, N., Nathan, R., Adamiec, G. & Lefrais, Y. 2012b: On the use of the infinite matrix assumption and associated concepts: A critical review. *Radiation Measurements 47*, 778-785.

Jacobs, Z., Duller, G. A. T. & Wintle, A. G. 2006c: Interpretation of single grain D_e distributions and calculation of D_e. *Radiation Measurements 41*, 264-277.

Jacobs, Z., Duller, G. A. T., Wintle, A. G. & Henshilwood, C. S. 2006a: Extending the chronology of deposits at Blombos Cave, South Africa, back to 140 ka using optical dating of single and multiple grains of quartz. *Journal of Human Evolution 51*, 255-273.

Jacobs, Z. & Roberts, R.G. (2015): An improved single grain OSL chronology for the sedimentary deposits from Diepkloof Rockshelter, Western Cape, South Africa. *Journal of Archaeological Science*: available online 18 February 2015.

Jacobs, Z. & Roberts, R. G. 2007: Advances in optically stimulated luminescence dating of individual grains of quartz from archeological deposits. *Evolutionary Anthropology 16*, 210-223.

Jacobs, Z., Roberts, R. G., Nespoulet, R., El Hajraoui, M. A. & Debénath, A. 2012: Single-grain OSL chronologies for Middle Palaeolithic deposits at El Mnasra and El Harhoura 2, Morocco:

Implications for Late Pleistocene human–environment interactions along the Atlantic coast of northwest Africa. *Journal of Human Evolution 62*, 377-394.

Lian, O. B. & Roberts, R. G. 2006: Dating the Quaternary: progress in luminescence dating of sediments. *Quaternary Science Reviews 25*, 2449-2468.

Løvborg, L. & Kirkegaard, P. 1974: Response of 3″ × 3″ NaI(Tl) detectors to terrestrial gamma radiation. *Nuclear Instruments and Methods 121*, 239-251.

Medialdea, A., Thomsen, K. J., Murray, A. S. & Benito, G. 2014: Reliability of equivalent-dose determination and age-models in the OSL dating of historical and modern palaeoflood sediments. *Quaternary Geochronology 22*, 11-24.

Mercier, N. & Falguères, C. 2007: Field gamma dose-rate measurment with a NaI(Tl) detector: re-evaluation of the "threshold" technique. *Ancient TL 25*, 1-4.

Murray, A. S. 1981: Environmental radioactivity studies relevent to Thermoluminescence dating. University of Oxford, Oxford.

Murray, A. S., Bowman, S. G. E. & Aitken, M. J. 1978: Evaluation of the gamma dose-rate contribution. *PACT 2*, 84-96.

Murray, A. S., Marten, R., Johnston, A. & Martin, P. 1987: Analysis for naturally occuring radionuclides at environmental concentrations by gamma spectrometry. *Journal of radioanalytical and nuclear chemistry 115*, 263-288.

Murray, A. S. & Roberts, R. G. 1997: Determining the burial time of single grains of quartz using optically stimulated luminescence. *Earth and Planetary Science Letters 152*, 163-180.

Murray, A. S. & Roberts, R. G. 1998: Measurement of the equivalent dose in quartz using a regenerative-dose single-aliquot protocol. *Radiation Measurements 29*, 503-515.

Murray, A. S., Roberts, R. G. & Wintle, A. G. 1997: Equivalent dose measurement using a single aliquot of quartz. *Radiation Measurements 27*, 171-184.

Murray, A. S. & Wintle, A. G. 2000: Luminescence dating of quartz using an improved single-aliquot regenerative-dose protocol. *Radiation Measurements 32*, 57-73.

Murray, A. S. & Wintle, A. G. 2003: The single aliquot regenerative dose protocol: potential for improvements in reliability. *Radiation Measurements 37*, 377-381.

Nathan, R. P. & Mauz, B. 2008: On the dose-rate estimate of carbonate-rich sediments for trapped charge dating. *Radiation Measurements 43*, 14-25.

Nathan, R. P., Thomas, P. J., Jain, M., Murray, A. S. & Rhodes, E. J. 2003: Environmental dose rate heterogeneity of beta radiation and its implications for luminescence dating: Monte Carlo modelling and experimental validation. *Radiation Measurements 37*, 305-313.

Roberts, R. G., Galbraith, R. F., Olley, J. M., Yoshida, H. & Laslett, G. M. 1999: Optical dating of single and multiple grains of quartz from Jinmium rock shelter, Northern Australia: Part II, results and implications. *Archaeometry 41*, 365-395.

Thomsen, K. J., Murray, A. S. & Bøtter-Jensen, L. 2005: Sources of variability in OSL dose measurements using single grains of quartz. *Radiation Measurements 39*, 47-61.

Wintle, A. G. 1997: Luminescence dating: laboratory procedures and protocols. *Radiation Measurements 27*, 769-817.

Wintle, A. G. & Murray, A. S. 1997: The relationship between quartz thermoluminescence, photo-transferred thermoluminescence, and optically stimulated luminescence. *Radiation Measurements 27*, 611-624.